REPORT DOCUMENTATION PAGE

Form Approved OMB No. 0704-0188

1. REPORT DATE *(DD-MM-YYYY)*	2. REPORT TYPE	3. DATES COVERED *(From – To)*
07-04-2010	Final Report	1 February 2009 - 01-Feb-10

4. TITLE AND SUBTITLE

Characterization of Ultra High Temperature Ceramics via Transmission Electron Microscopy

5a. CONTRACT NUMBER
FA8655-09-M-4002

5b. GRANT NUMBER

5c. PROGRAM ELEMENT NUMBER

6. AUTHOR(S)

Dr. Diletta Sciti

5d. PROJECT NUMBER

5d. TASK NUMBER

5e. WORK UNIT NUMBER

7. PERFORMING ORGANIZATION NAME(S) AND ADDRESS(ES)

National Research Council-CNR
Via Granarolo 64
Faenza 48018
Italy

8. PERFORMING ORGANIZATION REPORT NUMBER

N/A

9. SPONSORING/MONITORING AGENCY NAME(S) AND ADDRESS(ES)

EOARD
Unit 4515 BOX 14
APO AE 09421

10. SPONSOR/MONITOR'S ACRONYM(S)

11. SPONSOR/MONITOR'S REPORT NUMBER(S)
SPC 09-4002

12. DISTRIBUTION/AVAILABILITY STATEMENT

Approved for public release; distribution is unlimited.

13. SUPPLEMENTARY NOTES

14. ABSTRACT

Zirconium and hafnium diborides and carbides belong to the class of materials defined UHTCs (Ultra-High-Temperature-Ceramics). These materials are of particular interest because of the excellent and unique combination of properties which make them attractive candidates for high temperature applications where corrosion-wear-oxidation resistance are demanded. So far, the effort of the scientific community has been mainly directed to the study of processing procedures to improve the densification of these compounds. As very refractory compounds, these materials are very difficult to sinter to full density and temperatures as high as 2000-2400 degC and pressureassisted techniques are required to achieve dense materials. The addition of sintering aids has represented a strategy to overcome the intrinsic low sinterability of these highly refractory compounds. However the reaction between sintering additives, the matrix and its oxides (ZrO2, HfO2, B2O3..) during the high temperature stage leads to formation of intergranular phases and/or solid solutions, which, in turn affect the high temperature properties. The control of secondary phases composition is therefore of paramount importance for tailoring the performance of these materials. As there is still lack of knowledge on these microstructural aspects, the main aim of this work was to characterize Ultra-High-Temperature-Ceramics via electron microscopy techniques.

15. SUBJECT TERMS

EOARD, ultra high temperature ceramics, sintering

16. SECURITY CLASSIFICATION OF:			17. LIMITATION OF ABSTRACT	18, NUMBER OF PAGES	19a. NAME OF RESPONSIBLE PERSON
a. REPORT	b. ABSTRACT	c. THIS PAGE			WYNN SANDERS, Maj, USAF
UNCLAS	UNCLAS	UNCLAS	UL	44	19b. TELEPHONE NUMBER *(Include area code)* +44 (0)1895 616 007

istec

National Research Council

Institute of Science and Technology for Ceramics

European Office of Aerospace Research and Development
Bldg 186, Room 31
86 Blenheim Crescent
Ruislip, Middlesex HA4 7HB
United Kingdom

Faenza, January 21, 2010

Attn. Maj Wynn Sanders

OBJECT

II Technical report on: "Characterization of Ultra High Temperature Ceramic via Transmission Electron Microscopy"

Contract: FA8655-09-M-4002

Diletta Sciti
(Principal Investigator)

P.I. 02118311006
C.F. 80054330586

Via Granarolo, 64 – 48018 Faenza (RA) - ITALY
Phone: +39 0546 699711 - Fax +39 0546 46381
Administration Office *Fax: +39 0546 699719*
e-mail: irtec@irtec1.irtec.bo.cnr.it

FA8655-09-M-4002

Characterization of Ultra High Temperature Ceramics via Transmission Electron Microscopy - Part II: UHTCs sintered with addition of $TaSi_2$ -

Laura Silvestroni and Diletta Sciti

ISTEC-CNR, Institute for Science and Technology for Ceramics,

Via Granarolo 64

I-48018 Faenza, Italy

February, 2010

Table of Contents

List of Figures

Fig. 1: X-ray diffraction spectrum of the ZrB_2-15 vol% $TaSi_2$ composite. (a) 2θ: 20–70, (b) 2θ: 90–160°. Reflections from $CuKa_2$ radiation were removed.

Fig. 2: SEM images of the ZBT material: a) fractured surface and b) polished surface. In c) and d) the presence of secondary phases and solid solution is evidenced.

Fig. 3: Bright field TEM images showing a) a typical ZrB_2 grain surrounded by (Zr,Ta)B_2 solid solution, b) dislocations in the solid solution, c) a crystalline SiC particles within amorphous Si-O phase from which a dislocation departs and d) the $Ta_{4.8}Si_3C_{0.3}$ phase at the triple point.

Fig. 4: Bright field TEM images evidencing the dislocation chain at the interface between the core and the shell at low (a,b) and high (c) magnification. (d) Diffraction patterns showing epitaxy between core and shell.

Fig. 5: (a) Stacking faults in the solid solution, (b) interface between core and shell showing low angle grain boundary, (c) example of wetted grain boundary between two adjacent (Zr,Ta)B_2 grains.

Fig. 6: X-ray diffraction spectrum of the HfB_2-15 vol% $TaSi_2$ composite. (a) 2θ: 20–70, (b) 2θ: 94–106°. Reflections from $CuKa_2$ radiation were removed.

Fig. 7: SEM images of the HBT material: (a) fractured surface and (b,c,d) polished surfaces. Note in (b) the secondary phases and in (c) and (d) the (Hf,Ta)B_2 solid solution surrounding the original HfB_2 grains.

Fig. 8: Bright field TEM images showing the typical core- shell morphology of the HBT matrix with dislocation pile-up at the interface indicated by arrows in (a) and (b). Note in (c) Ta_5Si_3 at the triple point and the epitaxy between core and shell whose diffraction patterns are reported aside.

Fig. 9: (a) High-resolution TEM image showing an example of wetted grain boundary at the (Hf,Ta)B_2/$TaSi_2$ interface. (b,c) Twins crystallization in the Ta_5SiB_2 phase which displays non-wetting behavior towards the solid solution under this orientation.

Fig. 10: X-ray diffraction pattern for the HCT composite in the 2-theta range 70-120°. The underlying spectrum refers to pure HfC according to PDF# 39-1491.

Fig. 11: HfC-$TaSi_2$ composite: (a) fracture and (b,c) polished sections, (d) typical EDS spectra collected on HfC grains revealing the presence of Ta, (e) a Si-based phase.

Fig. 12: Bright field TEM images showing (a) dislocation activity between HfC-core and (Hf,Ta)-shell, (b) the $TaSi_2$ phase with low dihedral angles, (c-d) triple points along the matrix, (e) example of agglomerate of triple points with the corresponding EDS spectra.

Fig. 13: TEM images evidencing (a) dislocations pile-up, (b) clean grain boundary of the squared box in (a) between the solid solution and $TaSi_2$ and between two adjacent solid solution grains in (c). (d) Examples of EDS recorded on pure HfC and on two solid solutions, (e) Ta_5Si_3 phase located at the triple point and at the interface between two grains, (f) magnification of the squared area in (e) showing Moiré fringes in the solid solution.

Fig. 14: Magnification of some area of interest of the X-ray diffraction pattern for the HCT composite in the 2-theta range 40-105°. The overlapped peaks refer to stoichiometric TaC (PDF# 65-0282), $TaSi_2$ (PDF#65-3548) and Si standard (PDF#27-1402).

Fig. 15: TaC-$TaSi_2$ composite: (a) fracture and (b, c) polished sections.

Fig. 16: (a-c) Examples of shark-toothed interface between pure TaC-core and non stoichiometric TaC-shell. Ta_5Si_3 at the triple point in (d) and crystalline SiC among TaC matrixin (e). (f) Example of EDS recorded in the core and shell of TaC grain.

Fig.17: Molar content of the products deriving from the reactions: (a) 1 mol $TaSi_2$+1 mol CO(g), (b) 1 mol $TaSi_2$+1 mol B_2O_3, as a function of the temperature at constant pressure of 100 Pa.

Fig. 18: Sketch of the possible densification mechanisms occurring during sintering of UHTCs with addition of $TaSi_2$.

List of Tables

Summary

The microstructure of full dense hot pressed ultra-high-temperature ceramics, namely ZrB_2, HfB_2, HfC, and TaC doped with 15 vol% of $TaSi_2$, was characterized by x-ray diffraction, scanning and transmission electron microscopy.

Concerning the borides, the presence of carbides and oxide of the transition metals was observed well dispersed along the matrix of the composites. The ZrB_2 and HfB_2 grains displayed a core-shell structure: the core was constituted by the original MB_2 grain and the shell by a $(M,Ta)B_2$ solid solution which grew epitaxially on the core. The compositional misfit and the difference between the coefficient of thermal expansion between the core and the shell was accommodated by low angle grain boundaries and dislocations pile-up, especially pronounced in the ZrB_2-based composite, where a higher amount of Ta entered the lattice. At deeper investigations, Ta_5Si_3, $Ta_{4.8}Si_3C_{0.3}$ and Ta_5SiB_2, with Zr or Hf impurities were detected at the triple points. Wetting of the grain boundaries was observed. Based on the microstructural features, thermodynamical calculation and the available phase diagrams, it is suggested a densification assisted by a Ta-Si-O-B or -C liquid phase.

Also for the carbide-based systems, the formation of solid solution was confirmed. The surrounding (M,Ta)C solid solution was interfaced to the original MC grain by a shark toothed dislocation chain. At the triple point junctions $Ta_5Si_3C_x$ phases with Hf impurities were detected, but in this case the grain boundaries were clean.

The sintering mechanisms of early transition metals borides and carbides with addition of $TaSi_2$ as sinter-additive is reported in the present study, on the basis of the microstructural evolution observed upon sintering and in the light of phase diagrams and thermodynamical calculations.

The microstructure of the composites here presented are finally compared to composites sintered with addition of the same amount of $MoSi_2$.

1. Introduction

Zirconium, hafnium and tantalum diboride and carbide belong to the class of ceramic materials known as ultra-high temperature ceramics (UHTCs). These materials are of particular interest because of the unique combination of properties, such as high refractoriness, high electrical and thermal conductivity and chemical inertness against molten metals or nonbasic slags.[1–4] Applications that take advantage of these properties include refractory linings, electrodes, microelectronics, and cutting tools. Potential applications of these transition metals diborides and carbides also include aerospace manufacturing, for example, sharp leading edge parts on hypersonic atmospheric reentry vehicles, rocket nozzles and scramjet components, where the operating temperatures can exceed 3000°C.[1–4]

The major problems afflicting this class of material are related to the poor oxidation resistance in hypersonic environment, and the low fracture toughness (3-5 $MPam^{1/2}$), which is traduced in a unreliable behavior under severe thermal shock.

Much effort has been devoted in recent years to improve the densification and microstructure of these ultra refractory compounds, due to their high covalent bonds and low self-diffusion coefficient. Hot pressing at temperatures in the range 2200-3000°C is generally required for the densification of monolithic ZrB_2, HfB_2, HfC or TaC.[5-11] The temperature needed for densification can be strongly reduced (1400-1800°C) with small amounts of metallic or ceramic sintering additives such as Fe, Co, Mn, Ni or SiC, HfN, B_4C and C.[12-14] These additives are believed to favour the elimination of the surface oxides present on the starting particles which are supposed to hinder the matter transfer among the particles. However, the introduction of secondary phases often leads to grain coarsening, entrapped porosity, and low high temperature strength.

Previous studies have demonstrated that, besides SiC,[12] the addition of silicides, such as $MoSi_2$,[15–17] has positive effects on the densification and mechanical properties of borides and carbides, even at temperatures as high as 1500°C and without the application of pressure. In

addition, silicides, as silica-forming compounds, can offer significant improvement to the oxidation behavior.

Among the possibile additives that can meet the requirements imposed by the ultra-high environment, Ta-compounds are the most suitable, thanks to its high melting point, 2200°C, to the formation of a high melting oxide, Ta_2O_5 (1880°) and because Ta can stuff vacancies in Hf-, Zr- oxide and increase the immiscibility of the silica-based external glass, thus retarding the oxidation in the bulk.[18] Furthermore, the availability of Si-species which can form a protective silicon-based layer is desired upon oxidation.

So far, $TaSi_2$ has been employed for thin film applications in the field of electronics. Few data are available in the literature on the properties of polycrystalline $TaSi_2$ ceramics. $TaSi_2$ has a bulk density of 9.14 g/cm^3, hardness of 15.6 GPa, and is electrically conductive (electrical resistivity 50–55 mΩ·cm).[19] The elastic properties of $TaSi_2$ single crystals have been investigated by Chu et al.[20] who reported a room temperature Young's modulus of 360 GPa and Poisson's ratio of 0.189. Pastor and Meyer[21] first studied the effect of addition of $TaSi_2$ and other silicides on the densification and oxidation resistance of ZrB_2, assessing the formation of boride-silicide solid solutions and improvement of oxidation resistance in air up to 1200°C. Recently, Talmy et al.[22] have studied ceramics in the system ZrB_2–Ta_5Si_3 and have reported a significant improvement in the densification, which was fully accomplished at 1900°C and of the oxidation resistance in comparison with pure zirconium diboride. Furthermore, these authors have detected the formation of a ZrB_2-based solid solution phase, due to tantalum entering the diboride lattice. Opila et al.[23] studied the influence of $TaSi_2$ additions to ZrB_2–SiC compositions and found a significant improvement in the oxidation resistance at 1627°C in air. Finally, it was reported that $TaSi_2$ is beneficial as a sintering additive (2 vol%) for a HfB_2-based material,[24] due to liquid phase formation.

In this work, the effect of $TaSi_2$ addition on densification and microstructure evolution of some uhtcs, namely ZrB_2, HfB_2, HfC and TaC, is studied by scanning and transmisson

electron microscopy.

An overview of the microstructure and the mechanical properties of the compositions under exam are reported in [17] and [25], but a detailed characterization at nanoscale is still lacking.

Transmission electron microscopy (TEM) is a powerful tool to explore microstructures on a small length scale to disclose the densification mechanisms. This technique allows to acquire a variety of information with respect to microstructure and composition with high spatial resolution.[26] In order to tailor materials to meet specific requirements such as high temperature performance, the relationship between processing, microstructure, and mechanical behaviour has to be known and deeper investigations are mandatory. A thorough literature analysis revealed that very few detailed TEM works and reports on densification mechanisms are available for this class of materials, which however are essential to optimize the sintering aids utilized and the processing parameters applied.

2. Methods, Assumptions, and Procedures

The compositions under investigation are indicated in Tab. I. The commercial powders utilized for the materials production are reported in Tab. II. The powder mixtures were ultrasonically treated in absolute ethanol for 20 minutes and ball milled for 24 h using zirconia milling media, subsequently dried in a rotary evaporator and sieved to -60 mesh screen size.

Tab. I: Composition, sintering parameters, theoretical and experimental density, mean and maximum grain size of the $TaSi_2$-doped composites.

Sample	Composition (vol%)	Sintering (°C/min)	Ton (°C)	Th. density (g/cm^3)	Exp. density (g/cm^3)	M.g.s. (μm)	Max g.s (μm)
ZBT	ZrB_2-15 $TaSi_2$	1850/10	1580	6.5	6.5	2.0	4.6
HBT	HfB_2-15 $TaSi_2$	1900/15	1730	10.9	10.7	1.0	2.7
HCT	HfC -15 $TaSi_2$	1760/10	1600	12.1	12.0	0.8	2.2
TCT	TaC-15 $TaSi_2$	1750/9	1400	13.7	13.3	2.5	5.9

Tab. II: Characteristics of the commercial powders utilized for the production of the composites.

Powder	Crystal structure	Supplier	M.g.s. (μm)	Specific surface area (g/m^2)	Impurities (wt%)
$TaSi_2$	Hexagonal	ABCR, Gmbh & Co. Karlsrhue, Germany	<45	-	-
ZrB_2	Hexagonal	H.C. Starck, Karlsruhe, Germany, Grade B	<2	1.0	B: 18.7 C: 0.25 O: 2.0 N: 0.25 Fe: 0.1 Hf: 0.2
HfB_2	Hexagonal	Cerac Inc., Milwaukee, USA	2.19	1.38	Al: 0.001 Fe: 0.002 Z<0.5
HfC	Cubic	Cerac Inc., Milwaukee, USA	0.8	-	U: 0.0002 Zr: <0.6
TaC	Cubic	Cerac Inc., Milwaukee, USA	0.85	-	-

Some preliminary tests were carried out to attempt to pressureless sinter these materials but similar to results reported in the literature[21] compositions with 10 or 15 vol%$TaSi_2$ contained significant amounts of porosity (~10%), as ascertained by SEM analysis. Hot pressing was, therefore, chosen to densify the $TaSi_2$-contaning compositions. Hot pressing was conducted in low vacuum (~100 Pa) using an induction-heated graphite die with a constant uniaxial pressure of 30 MPa, heating rate 20°C/min and free cooling. For each composition, the maximum sintering temperature was set on the basis of the shrinkage curve, as indicated in Tab.I.

To identify the crystalline phases formed, all samples were examined using X-ray diffraction (Siemens D500, Karlsruhe, Germany), with CuK_α radiation, stepsize of 0.04 and 1 second counting rate.

The microstructures were analyzed on polished and fractured surfaces by scanning electron microscopy (SEM, Cambridge S360, Cambridge, UK) and energy dispersive x-ray spectroscopy (EDS, INCA Energy 300, Oxford instruments, UK). In order to limit lateral spreading of the electron beam, EDS analysis was carried out at acceleration voltages ≤6 KeV. TEM samples were prepared by cutting 3 mm discs from the bulk of the sintered pellets. These were mechanically ground down to about 20 μm and then further ion beam thinned

until small perforation were observed by optical microscope. Local phase analysis was performed using transmission electron microscopy (TEM) equipped with an energy-dispersive X-ray system (FEI, CM12, Eindhoven, The Netherlands; EDS, EDAX Genesis 2000, Ametek GmbH; Wiesbaden, Germany) operating at a nominal voltage of 120 keV. High-resolution investigations were performed using a FEI CM20 STEM operating at a nominal voltage of 200 keV. Quantitative calculations of the microstructural parameters, like residual porosity and secondary phase content, were carried out via image analysis with a commercial software package (Image Pro-plus 4.5.1. Media Cybernetics, Silver Springs, MD, USA). Thermodynamical calculations were performed using a commercial software HSC Chemistry for Windows 5, (Outokumpu Research Oy, Pori, Finland).

3. Results

3.1. ZrB_2- $TaSi_2$ composite

Hexagonal ZrB_2, hexagonal $TaSi_2$ and traces of tetragonal ZrO_2 were detected along with a series of reflections that were attributed to a solid solution formed by Ta diffusion into the ZrB_2 lattice (Fig. 1a). Compared with pure ZrB_2, these peaks were shifted towards higher angles, which indicates a contraction of the diboride unit cell. The unit cell parameters of this newly formed phase were a=3.152 Å and c=3.485 Å, i.e., shorter than those of pure ZrB_2 (a=3.169Å, c=3.530 Å). The shift was more pronounced at higher diffraction angles, as shown in the diffraction pattern of Fig. 1b. On the basis of the Vegard's rule, for the system ZrB_2–TaB_2 and hypothesizing that only Ta can enter the ZrB_2 structure, it can be estimated that the amount of Ta incorporated into ZBT was about 18–20 at.%, giving $(Zr_{0.8}Ta_{0.2})B_2$ as the composition of the solid solution.

Fig. 1: X-ray diffraction spectrum of the ZrB_2-15 vol% $TaSi_2$ composite. (a) 2θ: 20–70, (b) 2θ: 90–160°. Reflections from $CuKa_2$ radiation were removed.

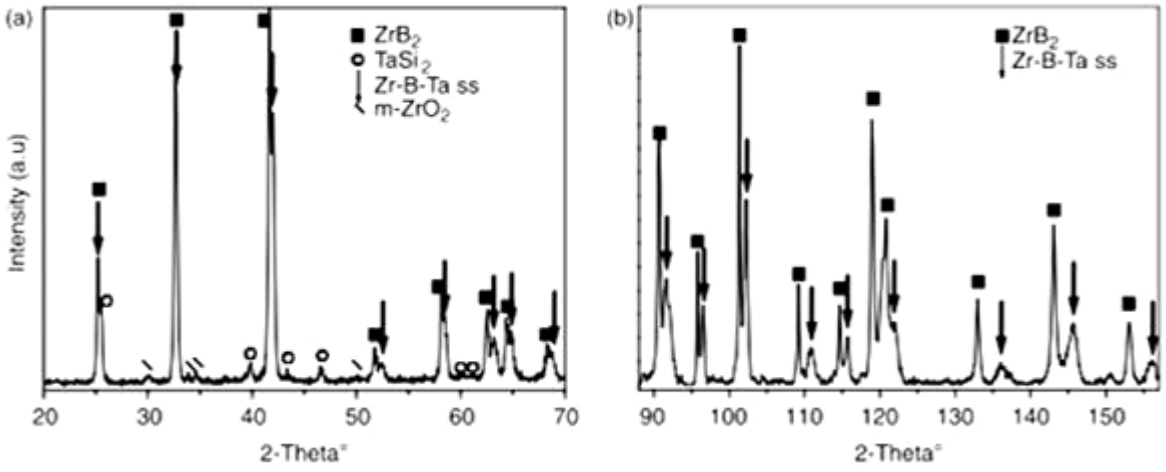

An example of the fracture surface of this composite is presented in Fig.2a. Little or no porosity (<1%) was observed, indicating that the relative density was higher than 99%. Some examples of polished surfaces of ZBT are shown in Fig. 2b-d. The globular ZrB_2 grains had an average size of about 2 μm. These grains were surrounded by a Zr–Ta–B solid solution, which appeared lighter in color (Fig. 2d). According to quantitative EDS analysis, the composition of this solid solution was $(Zr_{0.8}Ta_{0.2})B_2$ in agreement with the composition predicted by x-ray diffraction. Pure $TaSi_2$ was not clearly identified in the composite, but a Ta_xSi_y phase containing a certain amount of Zr was observed (Fig. 2d). This phase had a brighter color than ZrB_2 and $(Zr,Ta)B_2$. By image analysis, the content of the Ta_xSi_y phase was estimated to be 3–4 vol%. Residual ZrO_2 particles were also found along with silica-based phases containing various impurities. These oxide phases were attributed to the oxygen impurities in the starting powders and/or oxygen contamination during powder processing. Spurious carbide phases, such as Zr-Ta-C, SiC, or Si-C-O, were also detected in limited amounts (Fig.2c,d). Carbon enrichment could have resulted from the sintering environment and from the polyethylene bottles used for the milling procedure. Indeed, in the graphite- rich sintering environment, CO generation could have induced either the carburization of metals or the carbothermal reduction of oxide species.[27]

Fig. 2: SEM images of the ZBT material: a) fractured surface and b) polished surface. In c) and d) the presence of secondary phases and solid solution is evidenced.

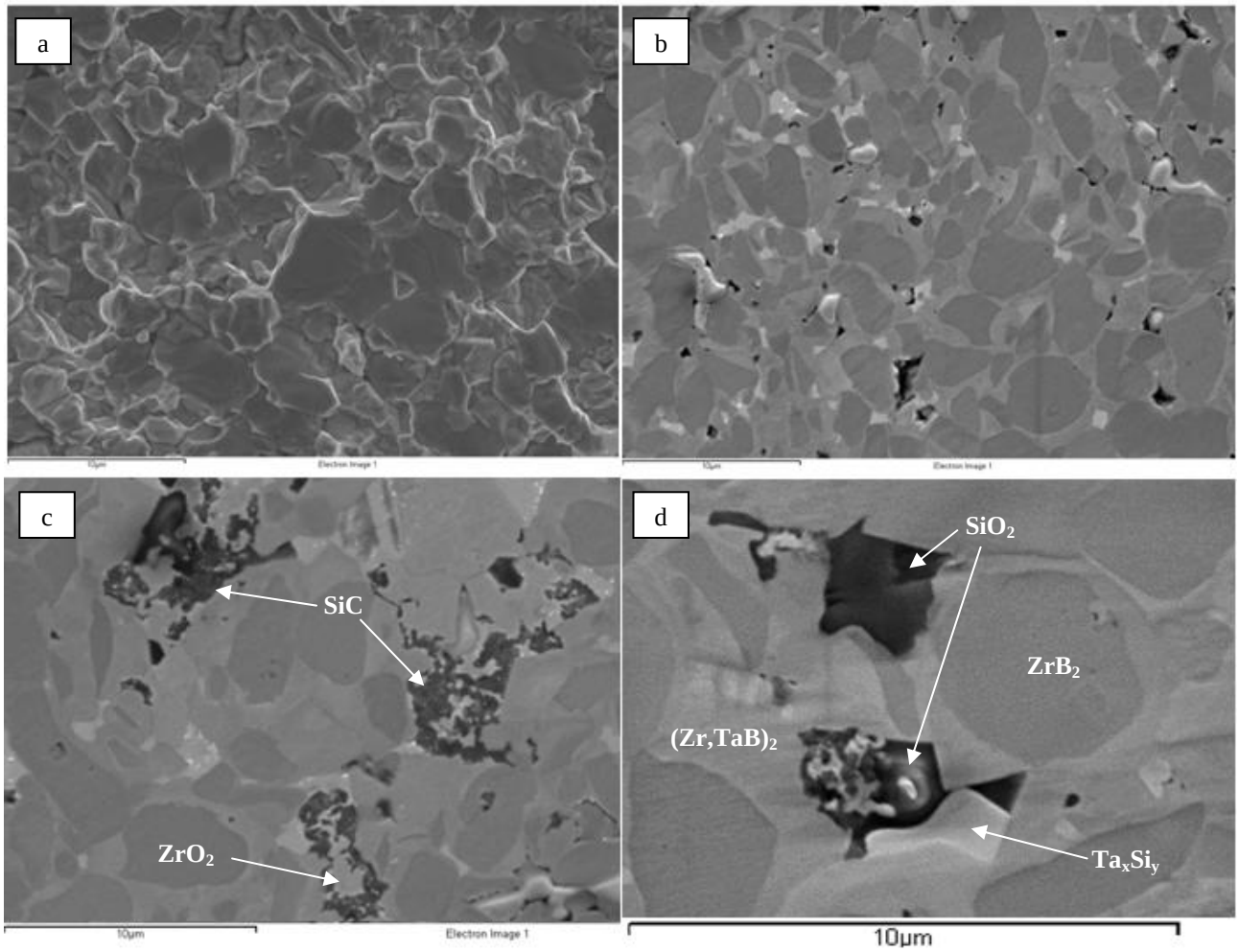

By TEM analysis the presence of the $(Zr_{0.8}Ta_{0.2})B_2$ shell surrounding the ZrB_2 core of the matrix was ascertained also by EDS. At the interface core/shell, a corrugate dislocation loop was systematically observed, as depicted in Fig.3a and generally the solid solution was rich of defective substructures as shown in Fig. 3b. A lively dislocation activity is showed in Fig.3c, where a crystalline SiC particle containing amorphous SiO_2 is also present.

By EDS analysis, Zr traces were detected in $TaSi_2$ and in SiO_2, on the contrary no Ta traces were identified in ZrO_2 or SiO_2, suggesting a discrete Zr solubility in the silica-based phases and confirming the Ta immiscibility.[28] In the $TaSi_2$ phase one third of Ta atoms were substituted by Zr, i.e. $(Ta_{0.7}Zr_{0.3})Si_2$. Further Ta-Si phases were detected at the triple junctions as $Ta_{4.8}Si_3C_{0.3}$ and Ta_5SiB_2. An example of such triple points is reported in Fig. 3d. Magnified

areas of the original ZrB_2 grain and the $(Zr,Ta)B_2$ solid solution are reported in Fig.4, where the diffraction patterns recorded in the core and the shell confirm the epitaxy between the two regions (Fig.4c,d).

Fig. 3: Bright field TEM images showing a) a typical ZrB_2 grain surrounded by $(Zr,Ta)B_2$ solid solution, b) dislocations in the solid solution, c) a crystalline SiC particles within amorphous Si-O phase from which a dislocation departs and d) the $Ta_{4.8}Si_3C_{0.3}$ phase at the triple point.

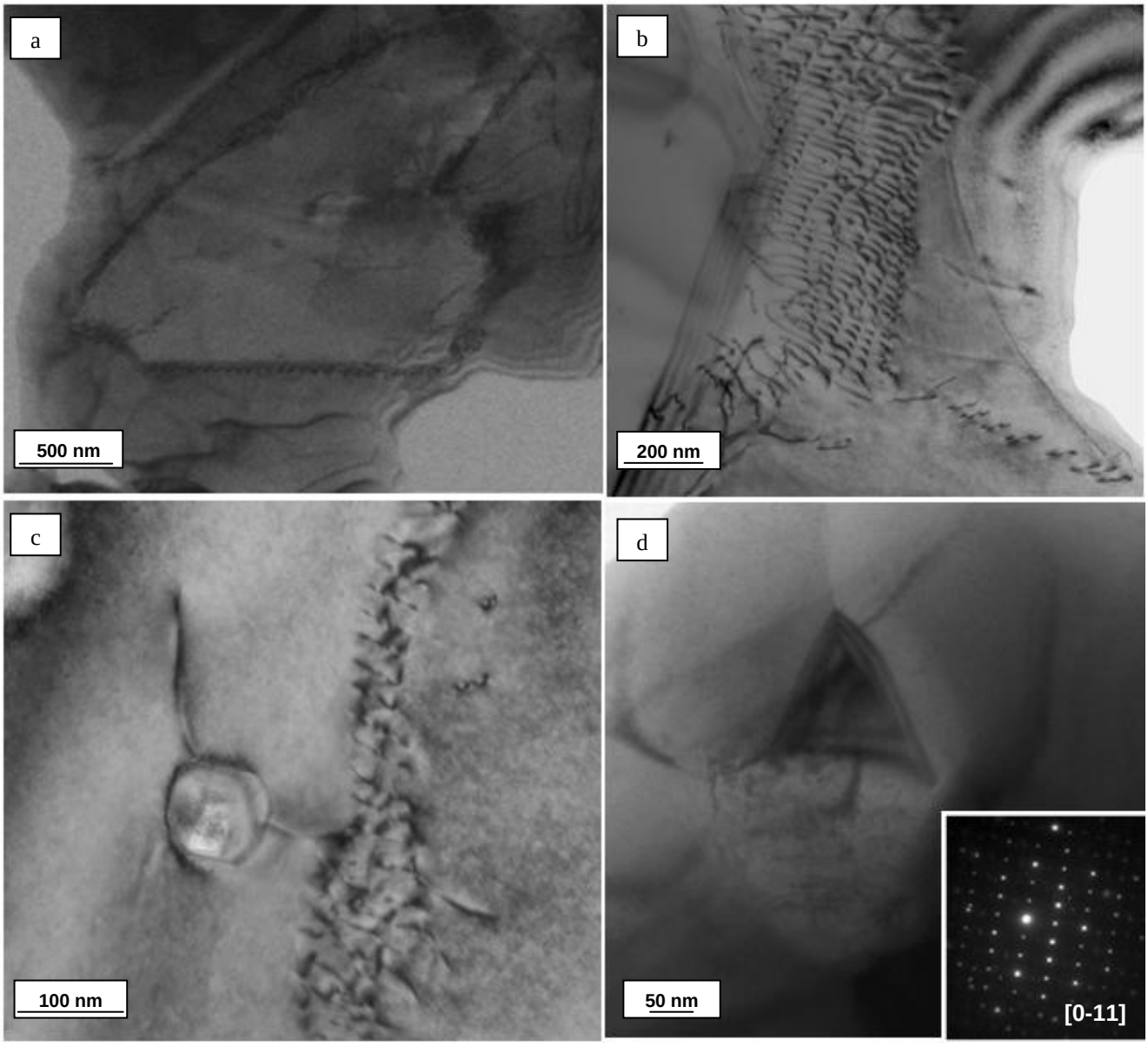

Fig. 4: Bright field TEM images evidencing the dislocation chain at the interface between the core and the shell at low (a,b) and high (c) magnification. (d) Diffraction patterns showing epitaxy between core and shell.

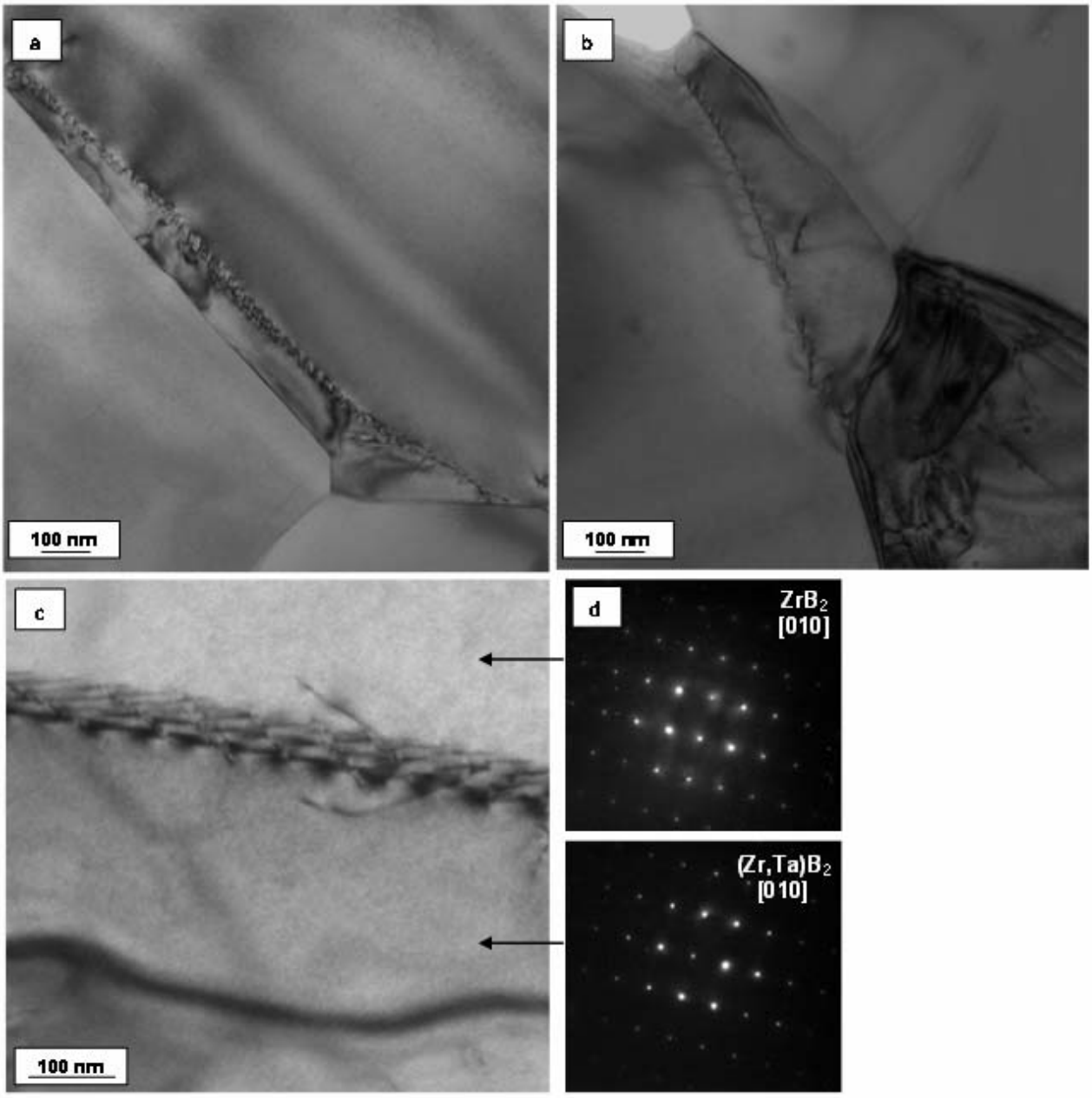

High-resolution TEM revealed the presence of low grain boundary lattice mismatch between core and shell, stacking faults in the solid solution, and an amorphous film between two adjacent solid solution (Fig.5), confirming a densification assisted by liquid phase. Since the solid solution is epitaxially oriented as respect to the original ZrB_2 grains, it is very probable that a Ta-Si-B-C-O liquid formed at the sintering temperature, ZrB_2 dissolved into the liquid

and reprecipitated upon cooling on the ZrB_2 seeds.

The core/shell contrast is hence due to the difference in chemical composition. The absence of abnormal grain growth means that no coalescence process occurred at the final stage of sintering.

Fig. 5: (a) Stacking faults in the solid solution, (b) interface between core and shell showing low angle grain boundary, (c) example of wetted grain boundary between two adjacent $(Zr,Ta)B_2$ grains.

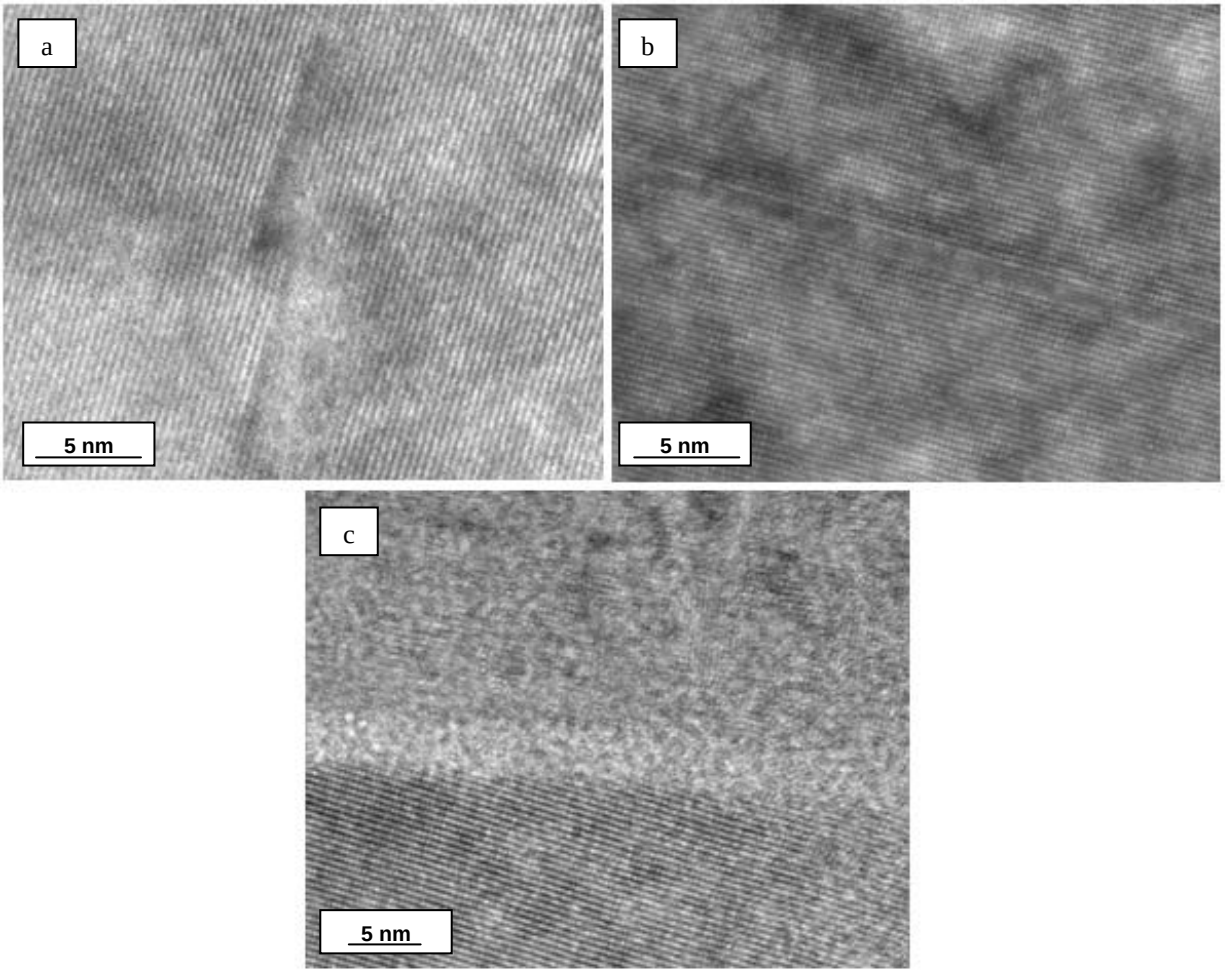

3.2. HfB_2-$TaSi_2$ composite

The XRD pattern indicated (Fig. 6) that mainly hexagonal HfB_2, hexagonal $TaSi_2$ and monoclinic HfO_2 were the crystalline phases. At high diffraction angles, splitting of the main reflections of HfB_2 was observed. Different from ZBT, the secondary peaks for HBT were visible only at high diffraction angles ($2\theta>90°$). These additional reflections were identified as a solid solution formed by the incorporation of Ta into the HfB_2 lattice. The unit cell

parameters of this newly formed phase were a=3.131 Å and c=3.440 Å, i.e., shorter than those of pure HfB_2 (a=3.140 Å, c=3.470 Å). According to the Vegard's rule applied to HBT, the amount of Ta incorporated into HBT was about 15–20 at.%, giving $(Hf_{0.8}Ta_{0.2})B_2$ as the composition of the solid solution.

Fig. 6: X-ray diffraction spectrum of the HfB_2-15 vol% $TaSi_2$ composite. (a) 2θ: 20–70, (b) 2θ: 94–106°. Reflections from $CuKa_2$ radiation were removed.

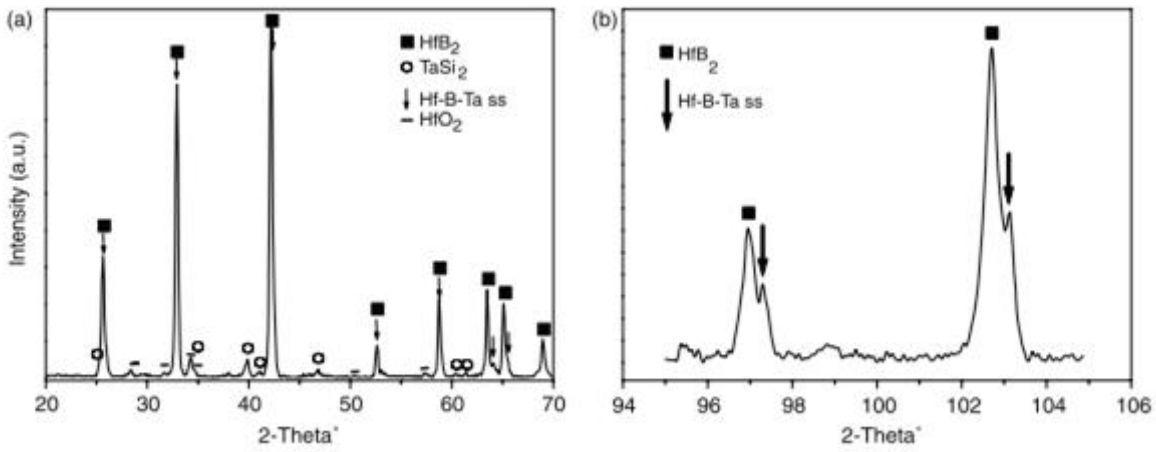

A fine microstructure with little porosity (<1%) was observed in HBT, see the fracture surface in Fig. 7(a). The mean HfB_2 grain size was around 1 μm, which was similar to the starting particle size of the HfB_2 powder, indicating that no significant grain coarsening occurred during sintering. The brightest phase was identified as HfO_2 in agreement with the findings of the X-ray diffraction pattern. Significant fractions of HfO_2 were found in other composites produced from the same starting HfB_2 powder as the present work,[15] suggesting a large oxygen contamination. $TaSi_2$ had a very irregular shape (Fig. 7d) and the way this phase filled the spaces between the HfB_2 grains indicated possible high-temperature ductile behavior. Other spurious phases were mixed carbides, based on (Hf,Ta)C and SiC, whose morphologies were consistent with a liquid-phase sintering mechanism. The origin of these carbides may be ascribed to the interaction of the sintering environment with the starting powders, as previously mentioned for ZBT. Analyzing the microstructure in BSE imaging, many HfB_2 grains exhibited a core-shell structure (Fig. 7c-d). By EDS analysis, the outer shell

was estimated to be a solid solution with composition $(Hf_{0.8}\ Ta_{0.2})B_2$ in agreement with the composition predicted by x-ray diffraction. The microstructural and XRD analyses showed that the formation of a solid solution was more pronounced in ZBT than in HBT, probably due to a higher Ta content in the boride lattice.

Fig. 7: SEM images of the HBT material: (a) fractured surface and (b,c,d) polished surfaces. Note in (b) the secondary phases and in (c) and (d) the $(Hf,Ta)B_2$ solid solution surrounding the original HfB_2 grains.

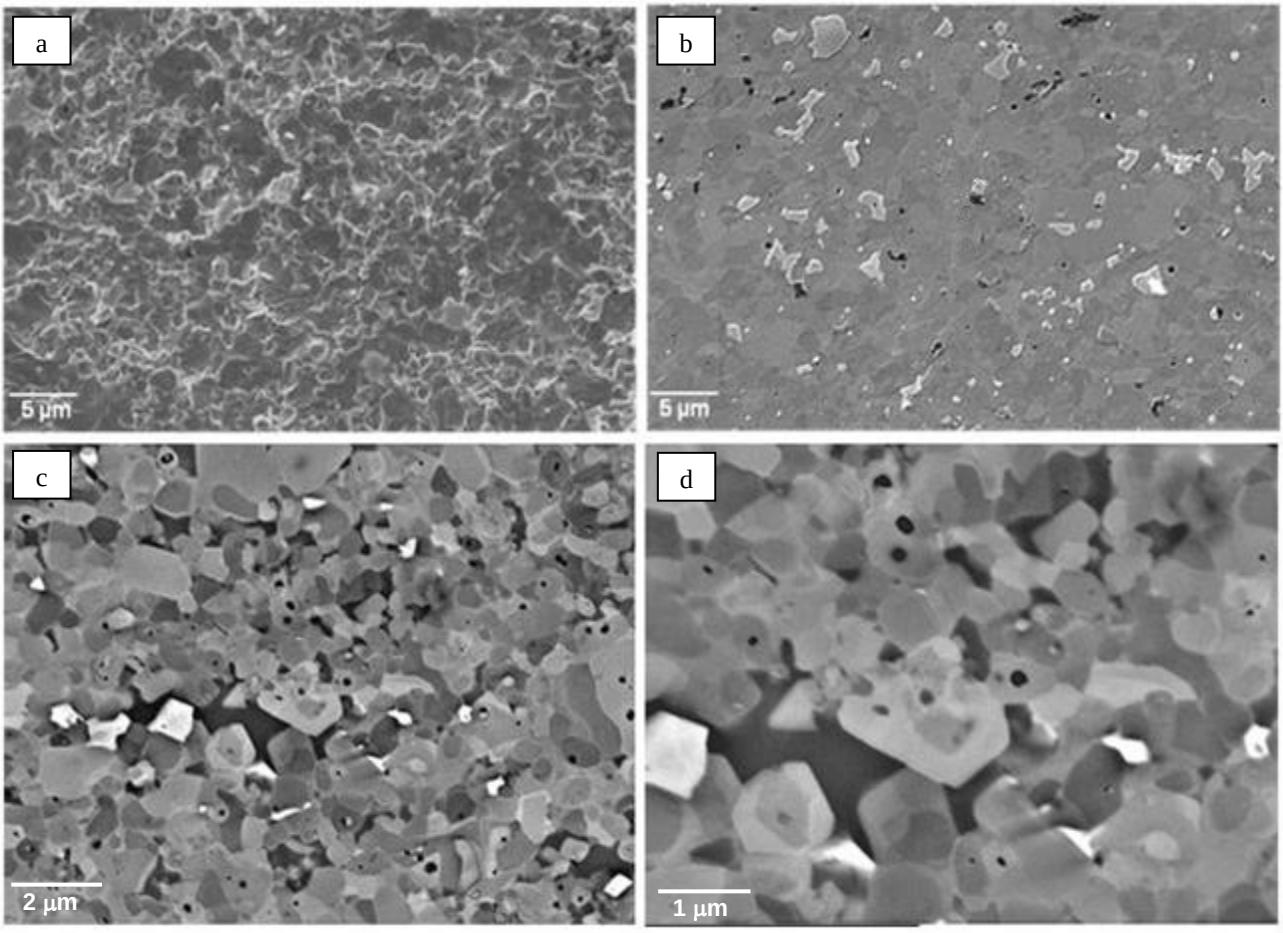

Higher magnification images recorded by TEM evidenced a rough interface between core and shell surrounding the core (Fig.8a-b), constituted by low angle grain boundary and dislocations loop, analogously to the ZrB_2-$TaSi_2$ system. These features suggested the existence of misfit strain at the interface, as a result of the compositional differences.

Also for this system, about one third of Ta atoms were substituted by Hf in the $TaSi_2$ phase, indicating that this silicide has a great solubility for the group IV metals. At the triple point junctions Ta_5Si_3 and Ta_5SiB_2 phases were detected (see Fig.8c). Also in this case core and

shell were epitaxial (Fig. 8d). In high resolution mode, the interface $(Hf,Ta)B_2/TaSi_2$ and $(Hf,Ta)B_2/Ta_5SiB_2$ were observed to be wet and clean, respectively, as indicated in Fig.9a-c. Twins were observed in Ta-Si-B phase, as shown in Fig.9c.

Fig. 8: Bright field TEM images showing the typical core- shell morphology of the HBT matrix with dislocation pile-up at the interface indicated by arrows in (a) and (b). Note in (c) Ta_5Si_3 at the triple point and the epitaxy between core and shell whose diffraction patterns are reported aside.

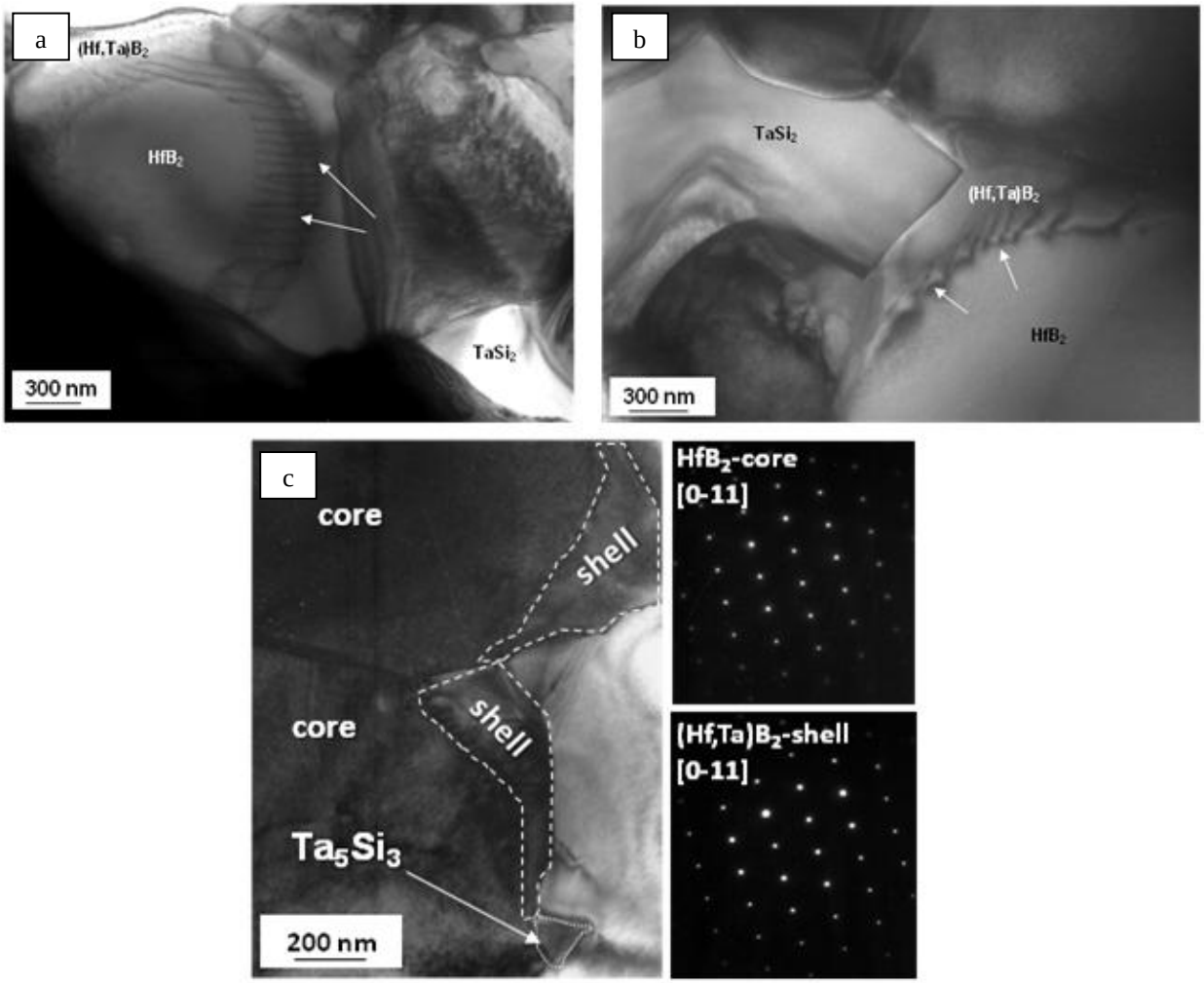

Fig. 9: (a) High-resolution TEM image showing an example of wetted grain boundary at the $(Hf,Ta)B_2/TaSi_2$ interface. (b,c) Twins crystallization in the Ta_5SiB_2 phase which displays non-wetting behavior towards the solid solution under this orientation.

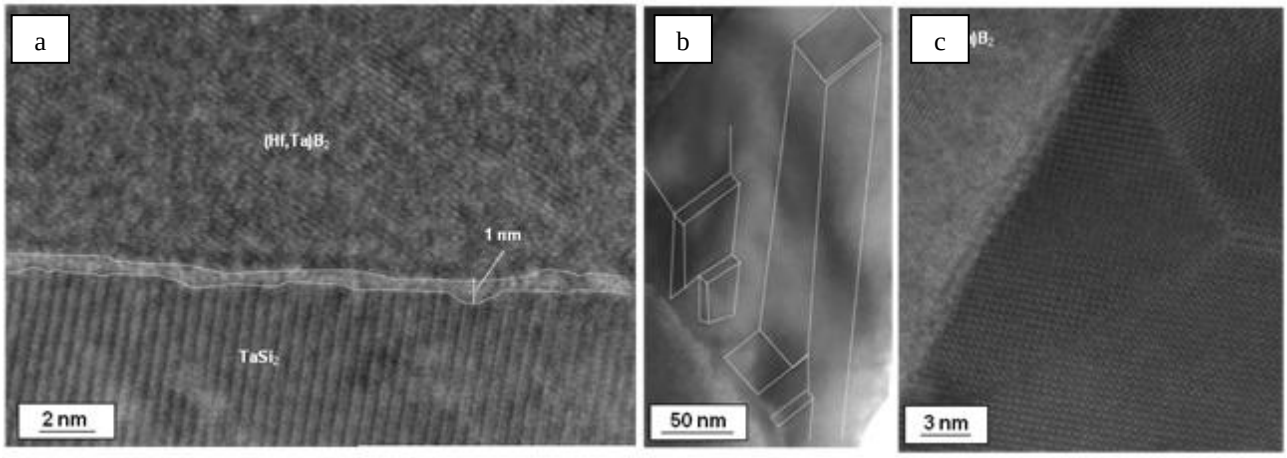

3.3. HfC-$TaSi_2$ composite

According to X-ray diffraction (Fig.10), no reflections from $TaSi_2$ were detected after sintering. Moreover, collected reflections do not correspond to those of pure HfC (PDF# 39-1491) being clearly shifted toward higher angles. This feature is displayed in the spectrum collected in the range 2θ=70-120°, where it was possible to distinguish at least two different peaks in each group of reflections, in addition to residual reflection from pure HfC. The unit cell parameters of these newly formed phases were a=4.623 and 4.420 Å, i.e. shorter than those of pure HfC (a=4.637 Å), which indicates a contraction of the unit cell. The presence of these additional reflections was interpreted as due to the formation of (Hf, Ta)C solid solutions. On the basis of the Vegard's rule for the HfC-TaC system and hypothesizing that only Ta can enter the HfC structure, it can be estimated that the amount of Ta incorporated into HfC grains was ~10 at% and ~20 at%, giving $(Hf_{0.9}Ta_{0.1})C$ and $(Hf_{0.8}Ta_{0.2})C$ as the compositions of the two identified solid solutions.

Fig. 10: X-ray diffraction pattern for the HCT composite in the 2-theta range 70-120°. The underlying spectrum refers to pure HfC according to PDF# 39-1491.

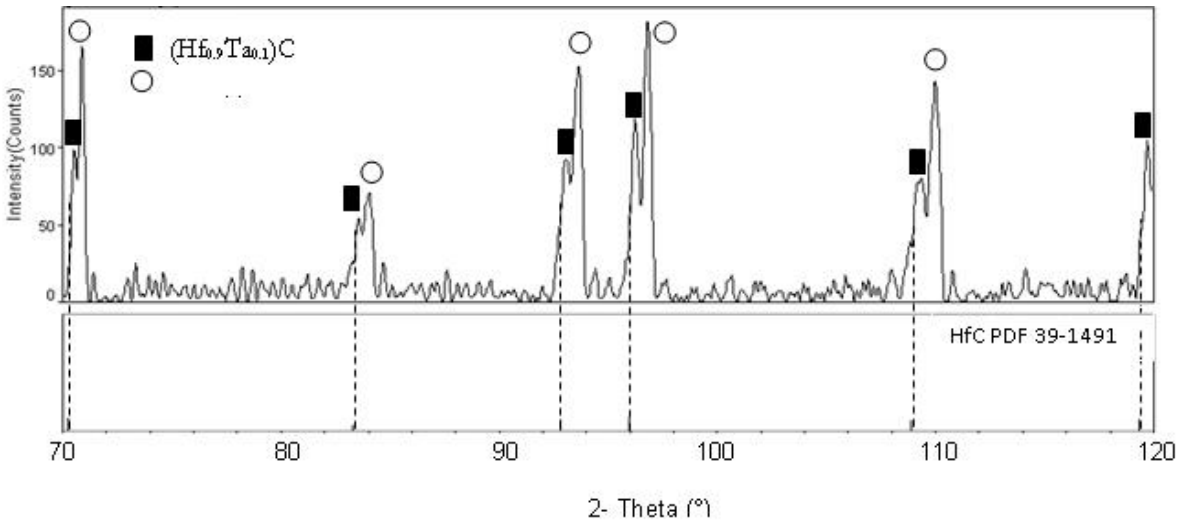

The microstructure of this composite (Fig.11.a,b) is fine and homogenous and the mean grain size of the HfC phase is of the order of 0.8 μm (Table I). Residual HfO_2 was also detected, due to oxygen contamination of the raw HfC powder (Fig. 11.c).

By EDS analysis, tantalum was confirmed to be present in most of the carbide grains (Fig.11.d). Residual secondary phases are less than 5 vol% and include unreacted $TaSi_2$ and Ta-Si-based phases whose composition is difficult to define. Occasionally, Si-based phases formed large pockets, as shown in Fig.11.e. When analyzed at very low accelerating voltage (EHT=5 keV) only the peaks of Si and C could be detected (see the inset in Fig.11.e). When the spectrum was collected at higher accelerating voltage (EHT=20 keV), additional peaks from Hf were also identified. This makes it difficult to ascertain if the C peak is collected from the underlying carbide matrix or not, i.e. whether the Si-based phase is silicon or SiC. As carbon sources are available in the present system, it is likely that a partial or complete carburization of silicon occurs.

Fig. 11: HfC-$TaSi_2$ composite: (a) fracture and (b,c) polished sections, (d) typical EDS spectra collected on HfC grains revealing the presence of Ta, (e) a Si-based phase.

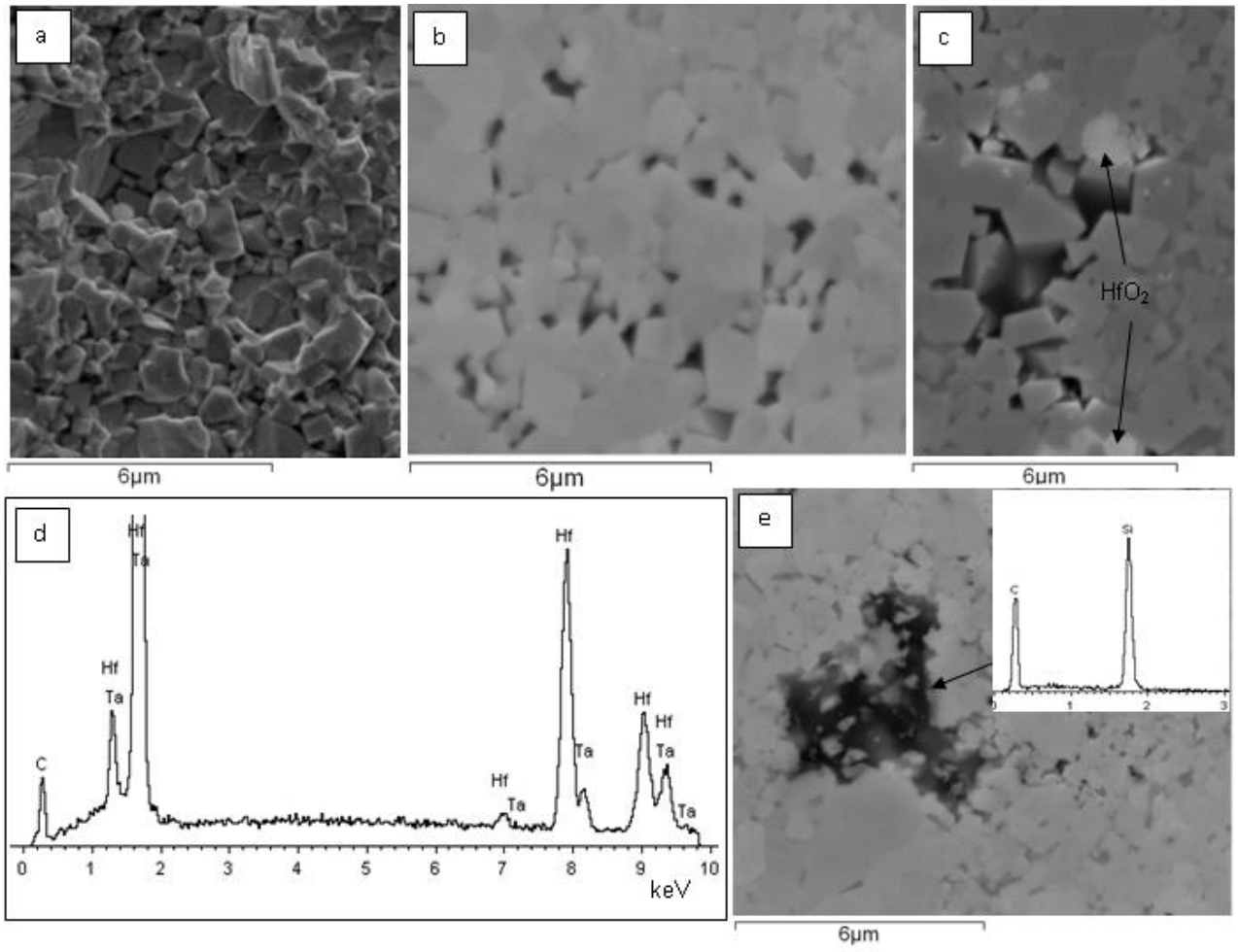

By TEM a dislocation activity and a core-shell structure were observed in HfC grains (Fig.12,13), the inner part was pure HfC and the outer part was a (Hf,Ta)C solid solution. At least two stoichiometries were measured by EDS, in agreement with the XRD findings. The subgrain morphology, not evidenced by SEM analysis, was revealed by TEM to be constituted by a dislocation pile up at the boundary between the pure phase and the solid solution.

Fig. 12: Bright field TEM images showing (a) dislocation activity between HfC-core and (Hf,Ta)-shell, (b) the $TaSi_2$ phase with low dihedral angles, (c-d) triple points along the matrix, (e) example of agglomerate of triple points with the corresponding EDS spectra.

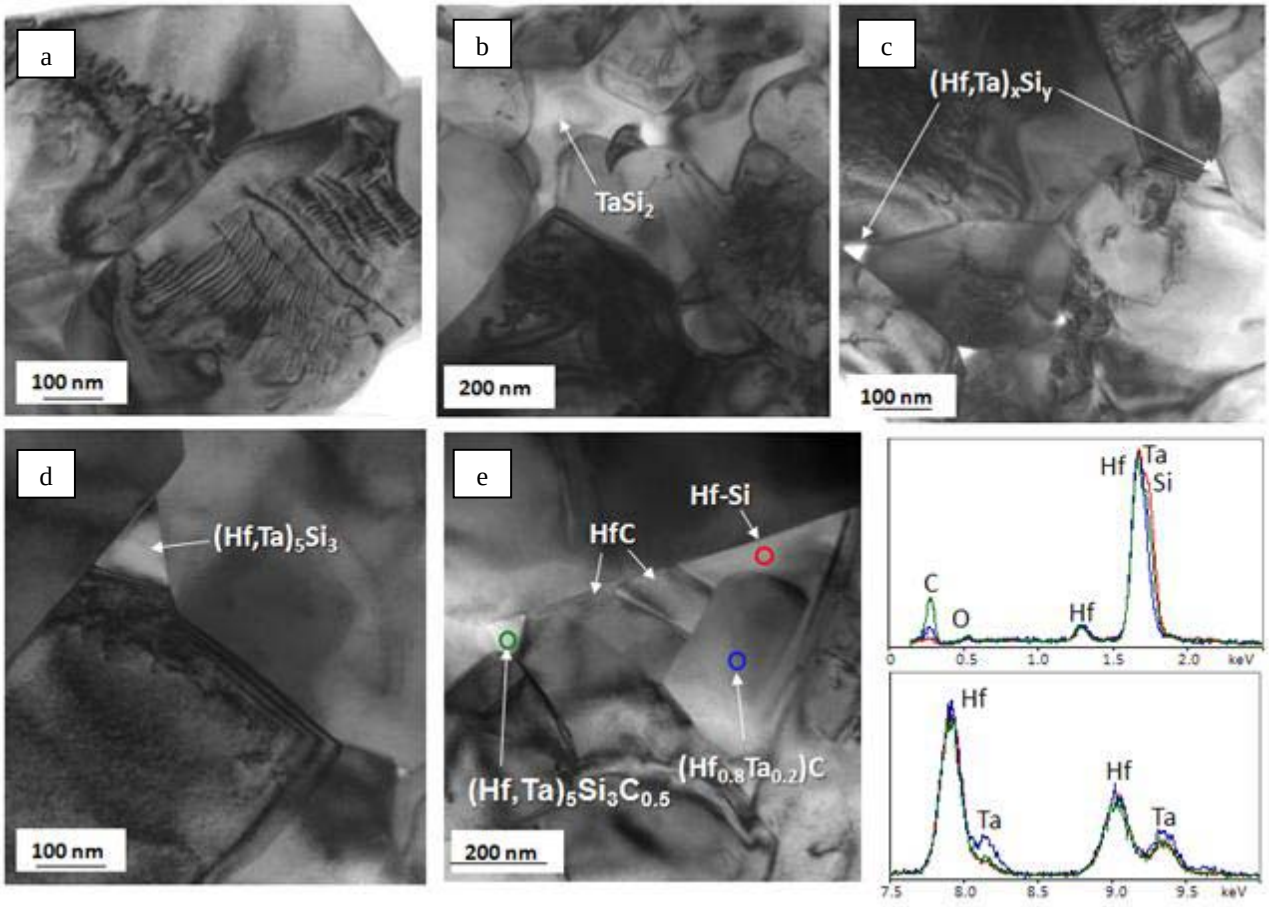

Besides $TaSi_2$ phase, recognizable as bright phase with irregular shape, accommodated among the HfC grains (Fig.12.b), $(Hf,Ta)_5Si_3$ and other mixed Hf-Ta-Si-C phases were detected at the triple point with bright contrast (Fig.12.c-e), about 50 nm big. The precise composition of these phase is difficult to detect, because Ta, Si and Hf have overlapping peaks in the range 1.5-2.0 keV. It is possible only to have a rough relative amount of the two

transition metals considering the peaks in the range 7.5-8.5 keV, however the amount of Si cannot be quantified due to its strong dependence on the thickness of the specimen and its strongest line overlapped to other elements present in the composite. On the other hand, the electron diffraction technique is too few imprecise to detect a lattice distortion in Ta_5Si_3 due to Hf substitution, considering that the two metals have very close atomic number.

High resolution studies revealed clean grain boundary both at the interface (Hf,Ta)C/(Hf,Ta)C and (Hf,Ta)C/$TaSi_2$ (Fig. 13).

Some defect image characteristics, such as Moiré fringes parallel to the operating reflection, dislocations and π-boundaries, are marked in Fig.13.e-f. The same defective structures were already observed in Si_3N_4 and SiAlONs during microstructural re-assessment.[29,30]

Fig. 13: TEM images evidencing (a) dislocations pile-up, (b) clean grain boundary of the squared box in (a) between the solid solution and $TaSi_2$ and between two adjacent solid solution grains in (c). (d) Examples of EDS recorded on pure HfC and on two solid solutions, (e) Ta_5Si_3 phase located at the triple point and at the interface between two grains, (f) magnification of the squared area in (e) showing Moiré fringes in the solid solution.

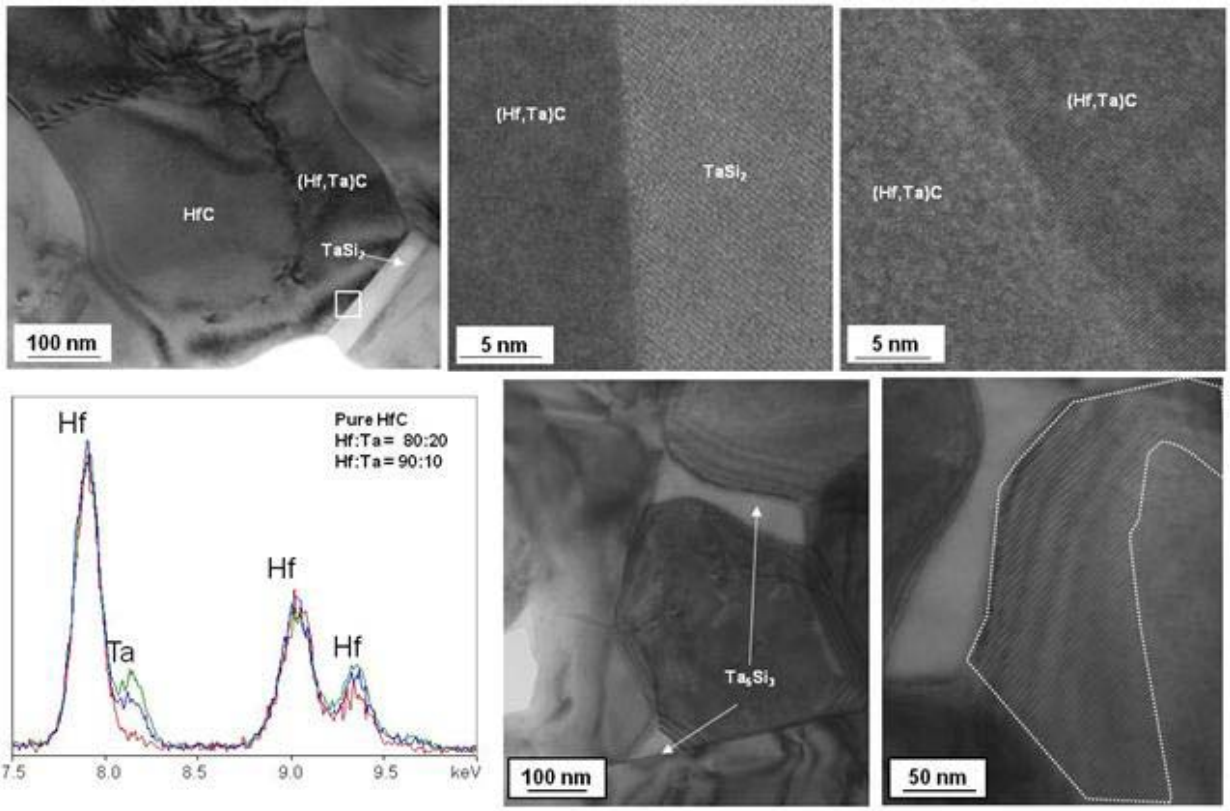

As previously reported by Hwang et al., these types of dislocation networks and Moiré fringes usually form when there is a rotational misfit between the core and the shell.[31] The

formation of the dislocation could be explained by rotational core/shell misfit, which probably resulted from the different thermal expansion due to their compositional difference.[32].

3.4. TaC-$TaSi_2$ composite

The x-ray diffraction pattern of this composite is reported in Fig.14; the analysis was performed with a Si standard in order to detect the eventual peaks shift. In the whole 2-Theta range, TaC and $TaSi_2$ are the only crystalline phases detected after sintering.

Fig. 14: Magnification of some area of interest of the X-ray diffraction pattern for the HCT composite in the 2-theta range 40-105°. The overlapped peaks refer to stoichiometric TaC (PDF# 65-0282), $TaSi_2$ (PDF#65-3548) and Si standard (PDF#27-1402).

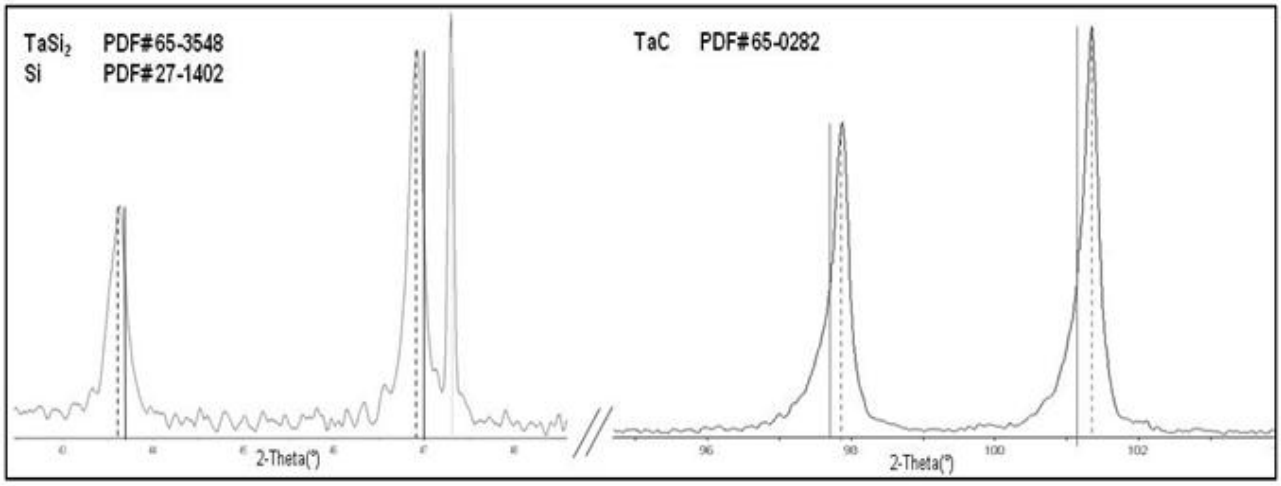

$TaSi_2$ peaks resulted shifted at lower angles, whilst TaC peaks at higher angles. This shift could be due to residual stress and/or to compositional modifications. The loss of carbon in the carbides decreases the lattice constants, while the strain relief increases these values.[33] The residual stress is related to the elastic moduli, the coefficient of thermal expansion and the volume fraction of the constituting phase. Due to the low amount of residual $TaSi_2$, i.e.~7 vol% calculated from x-ray diffraction pattern, and the approximation of the input values in Taya's formula,[34] low residual stresses are estimated, around -20 MPa for TaC and around 220 MPa for $TaSi_2$. For the matrix, the peak shift associated to such low value is well below the detection limit of the diffractometer, also considering the fact that a peak shift of 10^{-4} due

to residual stress of about 200 MPa in the composite ZrB_2-SiC is barely detectable.[35] On the other hand, a composition modification is very probable, due to the wide stability region of the fcc TaC_x phase. In particular, it is reported that carbon enrichment in the lattice leads to higher parameter.[33] Moreover it can be observed that all the peaks show asymmetry on the left side, which generally means the presence of lattice defects such as stacking faults, already observed in the solid solutions of the previous composites.

The fracture and polished surfaces, displayed in Fig.15, put in evidence little or no porosity. The fracture surface in Fig.15.a shows that larger grain (5-7 μm) are transgranularly fractured, whilst smaller grains (1-3 μm) are intergranularly fractured. The micrographs of the polished surface evidence that the mean grain size of the carbide phase is 2.5 μm, but coalescence of grains led to the formation of larger grains (up to 6-7 μm). $TaSi_2$ secondary phase is recognizable as having a slightly darker contrast compared to the matrix, and tends to form large pockets as wide as 3-8 μm (Fig.15.b). Moreover, it can be noticed that $TaSi_2$ phase have very low dihedral angles at the interface with the matrix, showing very ductile behavior. $TaSi_2$ is known to a have a brittle to ductile transition, similar to $MoSi_2$,[36] however, the high wettability displayed by the silicide could also be due to local liquid phase formation. According to image analysis, the volumetric amount of $TaSi_2$ in the final microstructure is around 10 vol%, i.e. slightly lower than the initial composition, 15%. Dark contrasting features were identified as SiC and SiO_2 phases (Fig.15.c).

By TEM inspections, a denticulate substructure can be observed in the matrix, analogously to the previous systems. Inner and external part are epitaxial and the corrugate feature of the sub-grain boundary denotes a lattice misfit (Fig.16.a-c). However, for this composite, the chemical analysis in the two regions is even more difficult, because from EDS we cannot say which is the stoichiometry of the TaC constituting the core and the shell, being carbon strongly dependent on the specimen thickness. The only assured composition difference between the two areas, is the presence of oxygen in the outer part, suggesting it can

derive from reprecipitation from a Ta-Si-C-O liquid phase (Fig. 16.f). At the triple point junctions Ta_5Si_3 and $Ta_{4.8}Si_3C_{0.3}$ were detected (Fig. 16.d-e).

Fig. 15: TaC-$TaSi_2$ composite: (a) fracture and (b, c) polished sections.

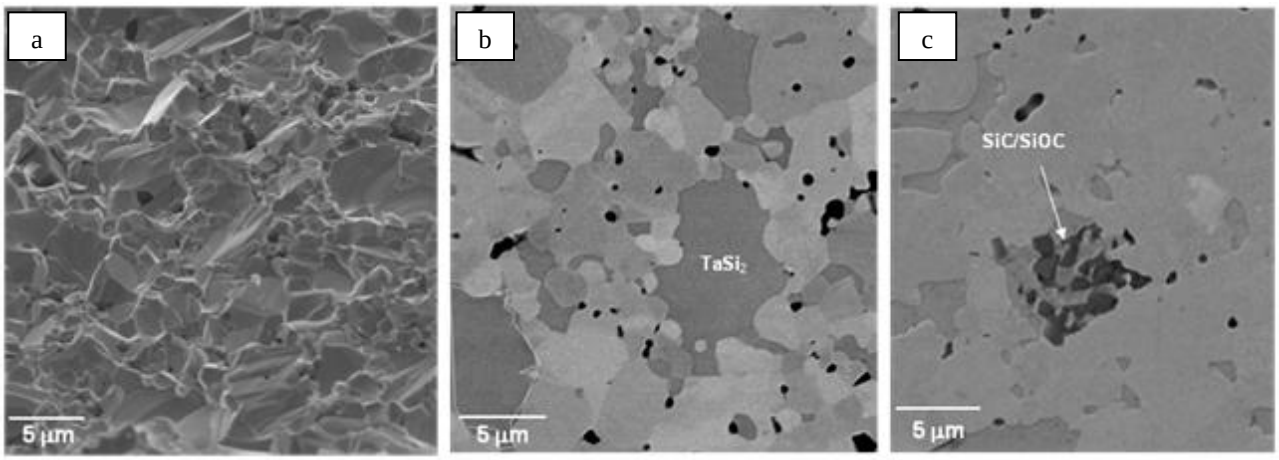

Fig. 16: (a-c) Examples of shark-toothed interface between pure TaC-core and non stoichiometric TaC-shell. Ta_5Si_3 at the triple point in (d) and crystalline SiC among TaC matrixin (e). (f) Example of EDS recorded in the core and shell of TaC grain.

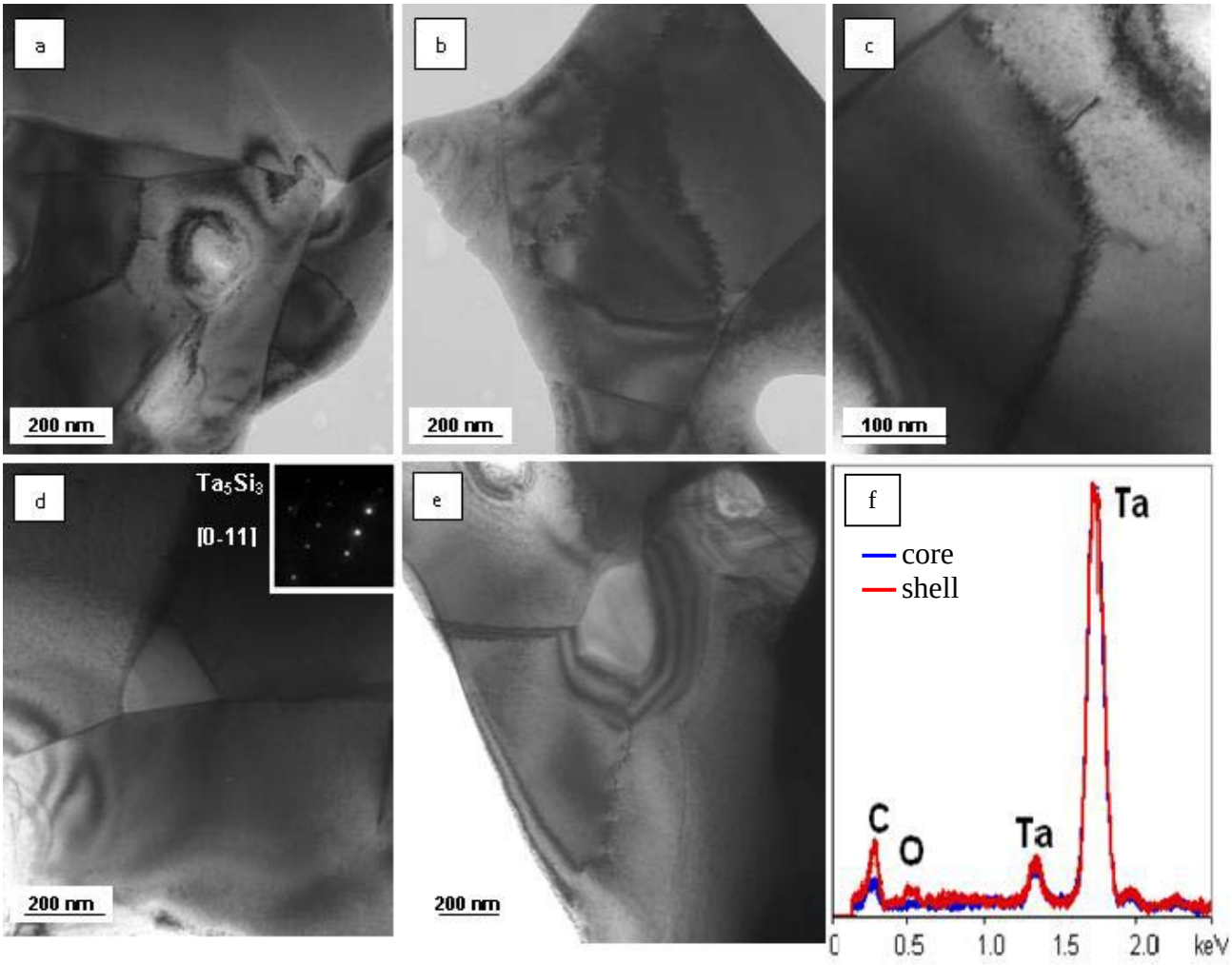

4. Discussion

As far as densification is concerned, different mechanisms are thought to occur for the compositions under investigation, however, in order to rebuild the active processes during sintering of borides and carbides of Zr, Hf and Ta with addition of $TaSi_2$, it is useful to summarize the main findings.

- In the case of the borides, the pressure increase during hot pressing of about 70 Pa in the temperature range 1300-1450°C and the weight loss after sintering, point out the formation of gaseous species.[25]
- The final microstructure of all the composites is characterized by the formation of Ta-containing solid solutions, which grew epitaxially on the matrix grain. The misfit between the core and the shell was accommodated by interfacial dislocation loop. This features evidence a discrete solubility of Ta in all the matrices.
- Investigations of the triple points revealed the formation further silicides, such as Ta_5Si_3 and Ta_5SiB_2 or $Ta_{4.8}Si_3C_{0.3}$, which contained Zr or Hf impurities. These features reveal a mututal solubuility of Zr and Hf in Ta-Si-based phases.
- High resolution TEM evidenced the presence of amorphous grain boundaries in the borides, whilst clean grain boundaries were observed in the carbides.

With the ambitious aim to figure out the path sequence leading to the final microstructure, several aspects of the densification process will be taken in exam.

4.1. Reactive environment

Let’s first investigate on the origin of the volatile species developed in the early stage of sintering.

The pressure increases in the hot press vacuum chamber recorded below 1400°C and the mass loss can be attributed to the development of gaseous species after interaction of $TaSi_2$ either with B_2O_3, which is present as surface oxide on the boride particles, or with CO

generated inside the graphite-rich environment of the furnace. Sources of carbon are easy to identify in the compositions investigated. Carbides are certainly C donors and further contamination may occur during sintering, which is conducted in a graphite-rich environment (graphite die and rams).

Using a commercial soft-ware package (HSC Chemistry for Windows 5, OutokumpuResearch Oy, Pori, Finland), some potential reactions between $TaSi_2$ and CO, or between $TaSi_2$ and B_2O_3 were analyzed in the range 1200–1900°C under a pressure of 100 Pa, i.e. approximately the vacuum level inside the hot-press chamber, considering pure phases with the activity of each phase equal to one. For simplicity, the molar ratio between the phases was taken equal to one. Molar products resulting from $TaSi_2$+CO and $TaSi_2$+ B_2O_3 reactions are displayed in Fig.17.

Fig.17: Molar content of the products deriving from the reactions: (a) 1 mol $TaSi_2$+1 mol CO(g), (b) 1 mol $TaSi_2$+1 mol B_2O_3, as a function of the temperature at constant pressure of 100 Pa.

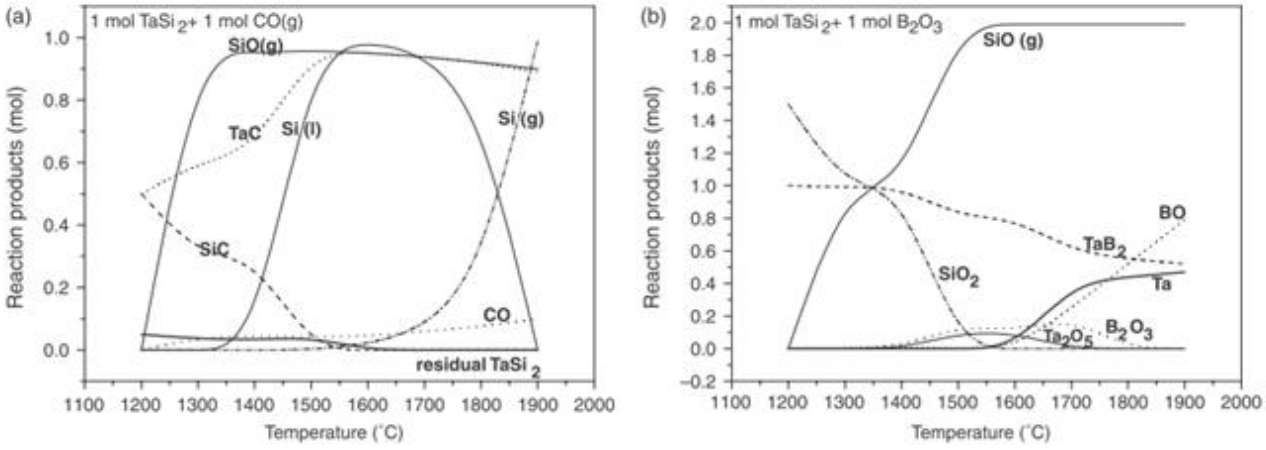

According to this thermodynamic analysis, it can be read that:

- CO promotes $TaSi_2$ decomposition with the formation of SiO gas at T≥1300°C and Si(g) at T≥1450°C. For T ≥1200°C, the formation of TaC and SiC is expected. In the range 1450–1850°C, the formation of liquid Si is predicted. The change in the Gibbs free energy varies from $-0.9 \cdot 10^3$ kJ at 1200°C to $-1.3 \cdot 10^3$ kJ at 1900°C.

- B_2O_3 too promotes $TaSi_2$ decomposition with the formation of SiO gas at T>1200°C, TaB_2 at T ≥1200°C and Ta at T ≥1700°C. At T ≥1400°C, the emission of BO also occurs. For this reaction the change in the Gibbs free energy varies from $-0.9 \cdot 10^3$ kJ at 1200°C to $-2.6 \cdot 10^3$ kJ at 1900°C.

The above thermodynamic predictions are in partial agreement with the microstructural observations and suggest that for both borides and carbides C and/or CO play a key role in the chemistry of these systems. $TaSi_2$ decomposition and consequent SiO volatilization was certainly confirmed by the weight loss, the pressure increase in the furnace chamber and microstructural analyses which revealed a lower amount of $TaSi_2$ compared to the initial content for all the composites.

From theses analyses it can be concluded that the most important reaction occurring during sintering of the $TaSi_2$-containing composites is:

$$TaSi_2 + CO(g) = TaC + 2\ Si(l) + SiO(g) \quad (1)$$

Since carbides are C donor and sintering is conducted in a C-rich furnace, carbon is the dominant moving species, so we can hypothesize the following reaction to occur:

$$Si(l) + C = SiC \quad (2)$$

Concerning the carbides, the newly formed TaC from reaction 1 can form solid solutions between HfC or the original TaC, which are completely soluble, according to:

$$TaC + HfC = (Hf_xTa_y)C \quad (3)$$

For the HCT composite, the occurrence of the above mentioned mechanisms is verified by the microstructural analyses. The reduction in the $TaSi_2$ content after sintering, as verified by X-ray diffraction, confirms the tendency to decomposition of this silicide. The formation of liquid silicon at relatively low temperature (reaction 1) is compatible with the enhanced sintering activity of the HfC-$TaSi_2$ compositions, with respect to other HfC-based ones. SiC phases deriving from carburization of silicon (reaction 2) are present in the microstructure (Fig.3.c, 11.e, 15.c). The formation of TaC was not observed, however, as it is well known

that the solubility between carbides of Group IV and monocarbides of Group V is complete and they are expected to form solid solutions.[37] The presence of (Hf, Ta)C solid solutions in the final microstructure confirms the occurrence of reaction 3.

In the TCT composite, TaC formation from reaction 1 is more difficult to track, as with the EDS technique it is tricky to detect stoichiometry difference between TaC-core and TaC-shell. However, also for this composite, Si-based phases are present in the microstructure and the final content of $TaSi_2$ is nearly a half of the starting composition.

For the borides a concurring reaction to reaction 1 is certainly:

$$TaSi_2 + B_2O_3 = TaB_2 + SiO(g) + SiO_2 \quad (4)$$

which has a negative Gibbs free Energy above 1000°C. No TaB_2 species were detected either by XRD or by electron microscopy analysis. However, these species are expected to form the solid solution with the borides. As confirmation of the occurrence of reaction 1 also in the borides, carbides formation, which were mixed phases of Ta and Zr or Hf, were observed in the final microstructure.

In both ZBT and HBT, Si-based phases with a very irregular morphology suggesting liquid-phase behavior were often detected. Possible origin of these phases can be either carburization of liquid silicon or carbo-thermal reduction of residual silica (Reactions 2, 4).

The possibility to have liquid phases during sintering is revealed by the irregular morphology of the silica-based phases, the negative curvature of residual $TaSi_2$ and the wet grain boundary in the boride-based composites.

From the densification behaviors, briefly summarized in Tab.I,[17,25] it is evident that the boride systems required higher maximum temperature and the shrinkage started at higher or equal temperature than the carbides. The enhanced densification behavior of $TaSi_2$ with the carbides, hence suggests that in the borides, reaction 4 occurred at a lower temperature then reaction 1.

4.2. Presence of liquid phases

From the previous paragraph, the main implication is that sintering is assisted by liquid phase. This hypothesis is further strengthened by the high wettability displayed by the $TaSi_2$ phase and the wet grain boundaries observed in the borides. Even the relatively high microstructural coarsening of the composites, as indicated in Tab.III., supports the formation of considerable amounts of liquid phases favoring matter transfer which drives grain growth and densification.

Tab. III: Comparison of the mean (m) and Max (M) grain sizes between hot pressed ceramics with addition of 15 vol% of $TaSi_2$ or $MoSi_2$. Δ% are referred to the starting powder dimensions. The sintering cycles are reported too in order to underline the eventual grain coarsening. For all the composites the same pressure was applied.

Sample	Sintering (°C,min)	Starting powder	m.g.s.	Δm.g.s. %	M.g.s.	ΔM.g.s. %
ZBT	1850/10	2	2	0	4.6	130
ZBM	1750/20	2	1.4	-30	4.5	125
HBT	1900/15	2.19	1	-54	3	37
HBM	1900/10	2.19	1.5	-32	2.5	14
HCT	1760/10	0.8	0.8	0	2.2	175
HCM	1900/10	0.8	1.2	50	2.3	188
TCT	1750/9	0.85	2.5	194	5.9	594
TCM	1850/3	0.85	1.2	41	3.7	335

In addition to the liquid silicon formed after reaction 1, others can be the sources of liquid that will be examined, according to the available phase diagrams.

The Ta-Si phase diagram[38] reports an eutectic point at 1400°C between $TaSi_2$ and Si, which is very probable to occur during decomposition of $TaSi_2$. One evidence of the formation of such liquid phase is the T_{ON} of the TCT composite (see Tab. I), which is exactly at 1400°C. In the same system, $TaSi_2$ and Ta_5Si_3 form an eutectic at 1970°C, which is yet above the maximum sintering temperature applied.

Subsequently, at temperature 1690-1700°C other eutectics are predicted between the Zr- and Hf- oxides and SiO_2, which covers the starting particles.[39, 40] Since Zr traces were detected in SiO_2 pockets by TEM-EDS, also this liquid cannot be ruled out. The corresponding Ta_2O_5-SiO_2 phase diagram[41] foresees an eutectic a 1887°C. This temperature is out of the sintering temperature range for the carbides (1750-1760°C), but very close to that of the borides (1850-1900°C).

Ta_2O_3 and B_2O_3 also form an eutectic point at 1700°C,[42] but since B_2O_3 is supposed to react with $TaSi_2$ (reaction 4), we can omit this equilibrium.

Besides these pseudo-binary systems, we do not have to forget important ternary systems, such as Ta-Si-B and Ta-Si-C.[43-45] Unfortunately, the position of the liquidus surfaces are not indicated for these systems, as only isothermal sections are presented to indicate the phases at equilibrium with one another. In addition, the same systems including oxygen, which would be of great help in better indentify the probable composition of the liquid phase, are to the best of the author's knowledge not available.

Hence we can just deduce from microstructural features what was the composition of the liquid phase. The crystallized triple points are Ta_5Si_3, Ta_5SiB_2 and $Ta_{4.8}Si_3C_{0.3}$ with M impurities, where M is the transition metal constituting the matrix, so we can assume a Ta-Si-B and/or -C based liquid where M is soluble. Moreover in the shell region, oxygen traces were also detected, that means this liquid took part in the removal of oxygen-bearing species from the particles surface.

4.3. Formation of solid solutions

The nature of bonding in the borides and carbides is known to be a mixture of covalent and metallic bonding with little ionic tendency. If solid solutions were formed, Ta substituted metal atoms in the carbides. According to Hume-Rotary rules, atomic size, electronegativity, electron valence and crystal structure are identified as important factors in solid solutions formation.[46] The size difference between guest and host must be below 15% for a solid solution to form. The IV^{th} and the V^{th} period metal atoms (Zr, Hf, Ta) have size factors even below 5% with tantalum, so this factor gives a positive indication on the possibility to have solid solution.

When a liquid volume fraction in liquid-phase sintered materials is sufficiently high for solid grains to be separated, dissolution-and –reprecipitation has been observed to occur

between the surface areas of a single grain, resulting in a corrugated solid-liquid interface. This phenomenon, which is referred to as an instability of the solid liquid interface" (ISLI), is known to occur when the compositional equilibrium between the grains and the liquid is broken by either changing the temperature or by introducing another element into the matrix.[47] It has been proposed that a solution layer, which forms at the initial stages of the equilibration reaction, remains coherent with the parent crystalline lattice until a critical thickness is achieved, and accumulates coherency strain energy. When the solution become thicker, it loses its coherency with the production of misfit dislocation, which is referred as coherency breaking, therefore no further migration is expected to occur.[48]

When a solid crystal is brought in contact with a liquid, its equilibration reaction occurs by two different processes: solution-reprecipitation and lattice diffusion in the crystal. The absence of inclusion at the interface core/shell might also suggest a diffusion process from the liquid phase, but a well defined boundary between core and shell suggests a reprecipitation from liquid phase. It is very likely that both the processes are active during densification.

Based on TEM observation, a schematic plot showing the hypothesized densification mechanism is reported in Fig.18.

Fig. 18: Sketch of the possible densification mechanisms occurring during sintering of UHTCs with addition of $TaSi_2$.

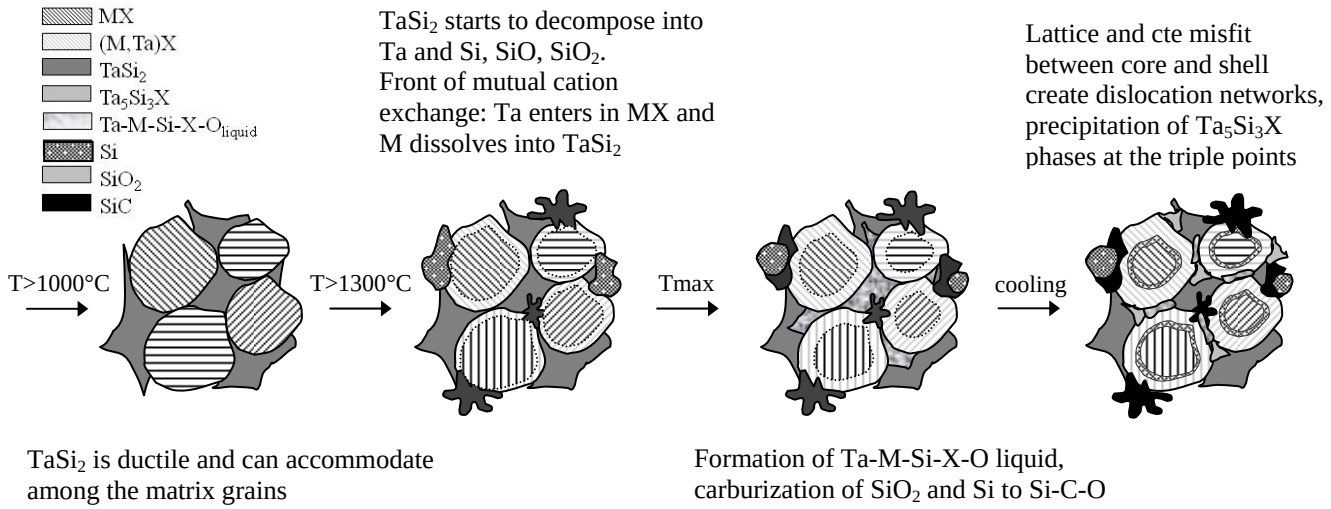

The matrix MX grain was initially surrounded by $TaSi_2$, which was ductile at temperature above 1000°C. At temperature above 1300°C and in presence of CO and/or B_2O_3, $TaSi_2$ started to decompose in Ta and $Si/SiO/SiO_2$. In this temperature range a front of mutual cations exchange formed: Ta diffused into ZrB_2 lattice and Zr diffused into $TaSi_2$. At the maximum temperature a TaSiBO/TaSiCO liquid phase, where the matrices are soluble in, was present. Some MX dissolved in the transient Ta-Si-B/C-O liquid phase and precipitated epitaxially on MX seed, as a result of the solution-precipitation process. In the first stage of densification a diffusion process is expect to prevail over the dissolution process, but at high temperature and when the thickness of the interexchange front reached a critical thickness, the dissolution process overcame the lattice diffusion.

Upon cooling, because of the compositional differences and the coefficients of thermal expansion misfit between the core and shell, dislocation loops, dislocation networks and Moiré fringes formed, as illustrated for example in Figs.12,13. Ta_5Si_3X phases, i.e. Ta_5SiB_2, $Ta_{48}Si_3C_{03}$, precipitated from the liquid phase at the triple points leaving an amorphous film in the borides or clean boundaries in the carbides.

Another source of stress which can induce lattice mismatch might be the crystallization of the triple points. Crystallisation of a glass, usually leads to a reduction in volume due to the closer packing of atoms in a crystalline structure, and it seems likely that a volume decrease will occur. Any volume change (increase or decrease) in the grain boundary phase will impose a strain on the matrix grains, deforming them and creating dislocations. Even if the extent of the defective area is quite enlarged and diffused to all the sample homogeneously, the presence of dislocation may be attributed also to this.[32]

For all the composites, the nonuniform Ta distribution was due to the fact that the processing time was not sufficient to allow for homogenization under the conditions used for densification. This feature is in agreement with the findings of Talmy et al.[22] for ZrB_2–Ta_5Si_3 composites.

4.4. Comparison with UHTCs sintered with addition of $MoSi_2$

In this section the microstructures just above presented will be compared to the microstructures of previously analyzed materials containing $MoSi_2$ as sintering additive sintered by hot pressing.[49,50] As far as it concerns $MoSi_2$-containing ceramics, TEM analysis were performed only on pressureless sintered materials.[16, 51] We are aware of the different sintering techniques, different sintering temperatures and holding time, however we believe some considerations can be done as well.

Decomposition of $TaSi_2$ and formation of liquid Si at relatively low temperatures can be considered the key events inducing the earlier densification of $TaSi_2$-containing composites compared to $MoSi_2$-containing ones. This leads to lower sintering temperature especially in the carbides, where the reducing environment, even C-richer due to the carbon release from the matrix, strongly favors $TaSi_2$ decomposition.

Another important aspect is the final grain size of the ceramics. In Tab. III the mean and maximum grain size of the 8 materials under examination are reported in comparison to the starting powders. We can observe that there is no significant difference between materials with the same matrix despite the same or lower temperatures were applied for $TaSi_2$-containing ceramics. This is particularly evident in the TaC-based materials: TCT was sintered at 100° lower than TCM, but the grain size was more than doubled. This feature evidences two main aspects. Firstly, the mechanism of mass transfer processes, both lattice diffusion and reprecipitation on the matrix seed, are far more active when $TaSi_2$ is used as sintering aid. Secondly, there is a higher mutual solubility of Ta in the matrix and of M in the liquid phase than Mo, probably also due to a higher approximation between the atomic radii.
For both sintering additives, the formation of mixed cations silico-borides and silico-carbides with stoichiometry 5:3 was found at the triple points. It seems assessed that this phase has a higher tendency to host interstitial cations, more than the silicides with stoichiometry 1:2,

hence the presence of this phase further increases the matter transfer and favors the formation of liquid phase at the eutectic composition.

Wetted interfaces were found for the borides with addition of either $MoSi_2$ and $TaSi_2$, where the grain boundary was constituted by residual Mo/Ta-Si-B-O liquid phase. On the contrary for the carbides, where the liquid phase at the sintering temperature was presumably constituted by Mo/Ta-Si-C-O, the interfaces matrix/matrix were observed to be cleaned.

High-temperature wettability is affected by a large number of variables that include temperature, contact time, atmosphere, roughness, crystal structure, composition, surface pretreatments and interfacial segregation, adsorption and reactions.[52] Basically, three types of interactions can promote wettability in the high-temperature solid-liquid systems: dissociation of surface oxides on liquid (oxide scavenging); chemical dissolution of the solid in the melt and interfacial adsorption of reactive solutes and formation of a wettable interfacial compound. At high temperatures, spreading to an equilibrium shape becomes difficult when a solid reaction product on the liquid opposes the spreading, resulting in a large value of the contact angle. The stability and protective influence of the oxide films are affected by the temperature, atmosphere and alloying elements. High temperatures decrease the liquid surface tension and promote wettability. Also, the spreading rate towards equilibrium is enhanced because of the diminishing liquid viscosity at high temperatures.[52] It is then evident that the removal of the oxide layer from the grains favor the wetting by means of the liquid phase.

We could try to explain the non wettability of the carbide phase hypothesizing that the liquid formed in the carbides had a higher viscosity than that formed in the borides and hence tended to solidify in discrete pockets rather than remaining trapped between two adjacent grains as amorphous film.

For metal systems, solid metals are perfectly wetted by their own melt. Several studies of wettability of solid metals by different liquid metals concluded that mutual solubility or formation of intermetallic compounds was a necessary condition for wetting.[53] If we try to

extend this condition to ceramics, we see that it is true in the case of borides, but not true for the carbides. For this last type of UHTCs other factors should be considered, however a systematic study of the wettability of these materials, although of paramount importance, is well beyond the scope of this study.

Finally, another striking difference between the groups of materials sintered with the two sintering additives is the formation of pile-up of dislocation at the core-shell interface in the $TaSi_2$-doped composites. This can be explained in terms of higher content of Ta in the solid solution, i.e. from XRD pattern 15 at% in the borides and 20 at% in HfC, compared to a nearly detectable amount of Mo, i.e. around 5 at%. To be precise, (Mo,M)C were not even detected neither by XRD or TEM analysis confirming a negligible solid solubility of Mo in transition metals carbides. On the contrary, (Ta,M)C were evidenced with TEM scrutiny. Higher content of Ta in the solid solution led to a more pronounced difference between the lattice parameters and the thermal expansion difference of core and shell, resulting in low angle grain boundaries and zips of dislocations.

A direct consequence of the presence of dislocations and sub-grains, is the enhancement of impurity or cations diffusion through the dislocation core. Diffusion through these short paths is 10^6 times faster than in the bulk.[54] This phenomenon too might have enhanced the mass transfer and hence the densification of $TaSi_2$-containing ceramics over $MoSi_2$-containing materials.

4. Conclusions

The microstructure of hot pressed borides of Zr and Hf, and carbides of Hf and Ta with addition of 15 vol% of $TaSi_2$ were studied through x-ray diffraction, scanning and transmission electron microscopy. $TaSi_2$ played an essential role in the densification through different mechanisms.

In reducing environment (C/CO-rich) or in presence of B_2O_3, $TaSi_2$ partially dissociates into Ta and $Si/SiO/SiO_2$ phases, which favour the formation of liquid phases where the matrices are partially soluble. For the borides the liquid was mainly constituted by Ta-Si-B-O, whilst for the carbide by Ta-Si-C-O. The former wetted the boride matrix, whilst the second crystallized at the triple points leaving clean grain boundaries of the carbides. The presence of traces of oxygen at the grain boundaries and at the triple junctions phases confirms that the liquid was effective in removing the oxide layer covering the starting powder, which is well known to hinder the densification of non-oxide ceramics. With respect to triple junctions, in all the composites Ta_5Si_3 was detected in addition to Ta_5SiB_2 in the borides and $Ta_{4.8}Si_3C_{0.3}$ in both the borides and the carbides.

All the composites presented a core/shell morphology type, where the core was constituted by the original grain, either MB_2 or MC, and the shell was a solid solution, $(M,Ta)B_2$ or (M,Ta)C.

At the interface core/ shell a dislocation loop was observed and, generally, many lattice defects were observed in the solid solution. The internal dislocation, π-boundary and Moiré fringes presumably formed to accommodate lattice mismatch and different coefficients of thermal expansion between the original core and the Ta-containing shell. The core/shell had the same orientation, suggesting that epitaxial growth started from the matrix seed and then eventually resulted in the core and shell structure.

Compared to $MoSi_2$, $TaSi_2$ showed to be more effective in enhancing the densification, thanks to its capability to form liquid phases at lower temperature and its higher mutual solubility with the matrices under examination.

Aknowledgements

One of the authors, L.S., wishes to express her gratitude to Hans-Joachim Kleebe for the useful suggestions and Mathis Müller for his precious help in TEM specimens' preparations.

References

1. L. E. Toth: Transition Metal Carbides and Nitrides, in Refractory Materials, A Series of Monographs, edited by J. L. Margrave (Academic Press Inc., New York, NY, 1971), pp. 6–10.
2. E. K. Storms: The Refractory Carbides, in Refractory Materials, A Series of Monographs, edited by J. L. Margrave (Academic Press Inc., New York, 1967), p. 94.
3. S. A. Shvab and F. F. Egorov: Structure and Some Properties of Sintered Tantalum Carbide. Sov. Powder Metall. Metal Ceram. 21, 894 (1982).
4. R. A. Cutler: Engineering properties of borides; in Ceramics and Glasses: Engineered Materials Handbook, Vol. 4. Edited by S.J. Schneider (ASM International, Materials Park, OH:, 1991), pp. 787-803.
5. M.Gasch, D.Elleby, E.I. Irby, S. Beckam, M.Gusman, S. Johnson: Processing, Properties and arc jet oxidation of hafnium diboride/silicon carbide ultra high temperature ceramics, *J. Mat. Sci.*, 39, 5925 (2004).
6. M.M. Opeka, I.G. Talmy, E.J. Wuchina, J.A. Zaykoski, S.J. Causey: Mechanical, Thermal, and Oxidation Properties of Refractory Hafnium and Zirconium Compounds, *J. Eur. Ceram. Soc.*, 19, 2405 (1999).
7. E. Wuchina, M. Opeka, S. Causey, K. Buesking, J. Spain, A. Cull, J. Routbort, F. Guitierrez-Mora, J. Mat. Sci. 39 5939 (2004).
8. A.L. Chamberlain, W.G. Fahrenholtz, G.E. Hilmas, D.T. Ellerby, J. Am. Ceram. Soc. 87 1170 (2004).
9. G. V. Samonov and R. Ya. Petrikina: Sintering of Metals, Carbides, and Oxides by Hot Pressing. Phys. Sintering, 2, 1 (1970).
10. J. S. Jackson: Hot Pressing High-Temperature Compounds. Powder Metall. 8, 73 (1961).
11. L. Ramqvist: Hot Pressing of Metallic Carbides. Powder. Metall. 9, 26 (1966).
12. E. Roeder, M. Klerk and Z. Metalkunde: Studies With the Electron-Beam Microanalyzer on Hot-Pressed Tantalum Carbide Having Small Additions of Manganese and Nickel. 54, 462 (1963).
13. X. Zhang, G.E. Hilmas, W.G. Fahrenholtz: Hot pressing of Tantalum Carbide with and without sintering additives. J. Am. Ceram. Soc. 90, 393 (2007).
14. W.G. Fahrenholtz, G.E. Hilmas, I.G. Talmy, J. A. Zaykoski: Refractory Diborides of Zirconium and Hafnium", J. Am. Ceram. Soc., 90, 1347 (2007).
15. L. Silvestroni, D. Sciti: Effects of $MoSi_2$ additions on the properties of Hf- and Zr-B_2 composites produced by pressureless sintering. Scirpta Mater. 57, 165 (2007).
16. L. Silvestroni, D. Sciti, J. Kling, S. Lauterbach, H. J. Kleebe: Sintering mechanisms of zirconium and hafnium carbides doped with $MoSi_2$. J. Am. Ceram. Soc. to be published (2009).
17. D. Sciti, L. Silvestroni, S. Guicciardi, D. Dalle Fabbriche, A. Bellosi: Processing, mechanical properties and oxidation behavior of TaC and HfC compositescontaining 15 vol% $TaSi_2$ or $MoSi_2$, Journal of Materials Research 24 [6] 1-10 (2009).
18. S. R. Levine, E. J. Opila: Tantalum Addition to Zirconium Diboride for Improved Oxidation Resistance, NASA/TM—2003-212483.
19. G. Schultes, M. Schmitt, D. Goettel, and O. Freitag-Weber: Strain Sensitivity of TiB_2, $TiSi_2$, $TaSi_2$ and WSi_2 Thin Films as Possible Candidates for High Temperature Strain gauges,' Sen. Actuators A, 126, 287–91 (2006).
20. F. Chu, M. Lei, S. A. Maloy, J. J. Petrovic, and T. E. Mitchell: Elastic Properties of C40 Transition Metal Disilicides,' Acta Mater., 44, 3035 (1996).
21. H. Pastor and R. Meyer: An Investigation of the Effect of Additions of Metal Silicides on Titanium and Zirconium Borides from the Point of View of their Sintering Behavior and their Resistance to Oxidation at High Temperature, Rev. Int. Htes Temp. Refract., 2, 41 (1974).
22. I. G. Talmy, J. A. Zaykovsi, M. M. Opeka, and A. H. Smith: Properties of Ceramics in the System ZrB_2–Ta_5Si_3, J. Mat. Res., 2, 2593 (2006).

23. E. Opila, S. Levine, and J. Lorincz: Oxidation of ZrB_2 and HfB_2-Based Ultra-High Temperature Ceramics: Effect of Ta Additions, J. Mat. Sci., 39, 5969 (2004).

24. F. Monteverde: Ultra-High Temperature HfB_2–SiC Ceramics Consolidated by Hot Pressing and Spark Plasma Sintering, J. Alloys Comp., 428, 197 (2007).

25. D. Sciti, L. Silvestroni, C. Melandri, G. Celotti, S. Guicciardi: Sintering and mechanical properties of ZrB_2-$TaSi_2$ and HfB_2-$TaSi_2$ ceramic composites, J. Am. Ceram. Soc. 91, 3285 (2008).

26. H. J. Kleebe, W. Braue, H. Schmidt, G. Pezzotti, G. Ziegler: Transmission electron microscopy in ceramic materials. J. Europ. Ceram. Soc. 16, 339 (1996).

27. R. M. German, in Sintering Theory and Practice, p. 432. John Wiley & Sons, Inc, New York, 1996.

28. I.G. Talmy, J. A. Zaykoski, M. M. Opeka: High temperature chemistry and oxidation of ZrB_2 ceramics containing SiC, Si_3N_4, Ta_5Si_3 and $TaSi_2$. J. Am. Ceram. Soc. 91, 2250 (2008).

29. M. Hwang, D.E. Laughling, I. M. Bernstein, Acta Metall. 28, 621 (1980).

30. S-L. Hwang, I-W. Chen, J. Am. Ceram. Soc. 77, 1719 (1994)

31. H.H. Lu, J. L. Huang: Microstructure in Silicon Nitride Containing b-phase seeding: III, grain growth and coalescence", J. Am. Ceram. Soc., 84, 1891 (2001).

32. W.E. Lee, G. E. Hilmas: Microstructural changes in ß-Si_3N_4 grains upon crystallizing the grain boundary glass, J. Am. Ceram. Soc., 72, 1931 (1989).

33. G. Santoro: Variation of some properties of Tantalum carbide with carbon content. Transactions of The Metallurgical Society of AIME, 227, 1361 (1963).

34. M. Taya, S. Hayashi, A.S. Kobayashi, H. S. Yoon: Toughening of a Particulate-Reinforced Ceramic-Matrix Composite by Thermal Residual Stress, J. Am. Ceram. Soc., 73, 1382 (1990).

35. F. Monteverde: The addition of SiC particles into a $MoSi_2$-doped ZrB_2 matrix: effects on the densification, microstructure and thermo-physiscal properties", Mat. Chem. and Physics 113, 626 (2009).

36. S. P. Simner, P. Xiao, B. Derby: Processing and microstructural characterization of RBSiC-$TaSi_2$ composites. J. Mat. Sci. 33, 5557 (1998).

37. H. O. Pierson: Handbook of Refractory Carbides and Nitrides. (William Andrew publishing/Noyes Westwood, New Jersey, USA, 1996) p. 68.

38. M.E. Schlesinger: The Si-Ta System, J. of Phase Equilibria, 15, 90 (1994).

39. N.A. Toropov, F.Y. Galakhov: Liquidation in the system ZrO_2-SiO_2. Uch. Zap. Kazan. Goa. Univ. 2, 158 (1965).

40. U.N. Parfenkov, R.G. Grebenshchikov, N.A. Toropov: Phase equilibrius in the hafniumdioxide-silicon dioxide system. Dokl. Akad. Nauk. SSSR 185, 840 (1969).

41. R.S. Roth, J.L. Waring, Phase Diagrams for Ceramists, Diagram 4448, (1970)

42. R.S. Roth, J.L. Wang, Phase Diagram for Ceramists, Diagram 4392, (1970)

43. H. Nowotny, R. Kieffer, F. Benesovsky: Silicoboride der übergangsmetalle Vanadin, Niob, Tantal, Molybdän und Wolfram, Planseeberichte für Pulvermetallurgie, 5, 86 (1957).

44. J.C. Schuster: Investigations in the ternary systems V-Si-C and Ta-Si-C, J. Chim. Phys. 90, 373 (1993),

45. A.I. Gusev: Phase equilibria in M-X-X' and M-Al-X ternary systems (M=transition metal;X,X'=B,C,N,Si) and the crystal chemistry of ternary compounds, Russian Chemical Reviews, 65, 379 (1996).

46. W. Hume-Rothery: Atomic Theory for Students of Metallurgy, Monograph and Report Series No. 3, The Institute of Metals, London, 1969.

47. J.H. Choi, D.Y. Kim: Instability of solid-liquid interfaces in magnesia single crystals, J. of Ceramic processing research, vol 4, 56 (2003).

48. M.S. Sulonen: Discontinuous mode of dissolution of a β phase precipitate into α Cu-Cd solid solutions, Acta Metall. 8, 669 (1960).

49. A. Balbo, D. Sciti: Spark plasma sintering and hot pressing of ZrB_2-$MoSi_2$ ultra-high-temperature ceramics, Mater. Sci. Eng. A 475, 108 (2008).

50. D. Sciti, L. Silvestroni, A. Bellosi: Fabrication and properties of HfB_2-$MoSi_2$ composites produced by hot pressing and spark plasma sintering, J. of Mater. Res. 21, 1460 (2006).

51. L. Silvestroni, D. Sciti, H-J. Kleebe, S. Lauterbach, M. Müller: Transmission Electron Microscopy on Zr- and Hf-borides Doped with $MoSi_2$: Densification Mechanisms, in press at the J. of Mater. Res.

52. N. B. Dahotre, P. Kadolkar, S. Shah: Refractory ceramic coatings: processes, systems and wettability/adhesion, Surf. and Interface Anal., 31, 659 (2001).

53. F. Delannay, L. Froyen, A. Deruyttere: The wetting of solids by molten metals and its relation to the preparation of metal-matrix composites composites, J. Mater. Sci. 1987 22, 1

54. I. Nöllmann, A. B. Trigubo, N. E. Walsöe de Reca: Subgrain structure and dislocation density in annealed MCT, Jap. J. of Appl. Physics, 30, 1787 (1991).

List of Symbols, Abbreviations, and Acronyms

TEM: Transmission electron microscopy

SEM: Scanning electron microscopy

M: transition metal, either Zr or Hf

X: B, C

ZBT: ZrB_2 + 15 vol% $TaSi_2$

HBT: HfB_2 + 15 vol% $TaSi_2$

HCT: HfC + 15 vol% $TaSi_2$

TCT: TaC + 15 vol% $TaSi_2$

ZBM: ZrB2 + 20 vol% $MoSi_2$

HBM: HfB2 + 20 vol% $MoSi_2$

HCM: HfC + 20 vol% $MoSi_2$

TCM: TaC + 20 vol% $MoSi_2$